The Company of Biologists

RESEARCH ARTICLE

Dynamic remodeling of ribosomes and endoplasmic reticulum in axon terminals of motoneurons

Chunchu Deng[1,*], Mehri Moradi[1,*], Sebastian Reinhard[2], Changhe Ji[1], Sibylle Jablonka[1], Luisa Hennlein[1], Patrick Lüningschrör[1], Sören Doose[2], Markus Sauer[2] and Michael Sendtner[1,‡]

ABSTRACT

In neurons, the endoplasmic reticulum (ER) forms a highly dynamic network that enters axons and presynaptic terminals and plays a central role in Ca^{2+} homeostasis and synapse maintenance; however, the underlying mechanisms involved in regulation of its dynamic remodeling as well as its function in axon development and presynaptic differentiation remain elusive. Here, we used high-resolution microscopy and live-cell imaging to investigate rapid movements of the ER and ribosomes in axons of cultured motoneurons after stimulation with brain-derived neurotrophic factor. Our results indicate that the ER extends into axonal growth cone filopodia, where its integrity and dynamic remodeling are regulated mainly by actin and the actin-based motor protein myosin VI (encoded by *Myo6*). Additionally, we found that in axonal growth cones, ribosomes assemble into 80S subunits within seconds and associate with the ER in response to extracellular stimuli, which describes a novel function of axonal ER in dynamic regulation of local translation.

This article has an associated First Person interview with Chunchu Deng, joint first author of the paper.

KEY WORDS: ER dynamics, Axon terminals, BDNF stimulation, Dynamics of local translation

INTRODUCTION

In neurons, the endoplasmic reticulum (ER) provides a luminal space throughout the cytoplasm, which extends into dendrites and axons (Terasaki et al., 1994; Wu et al., 2017). Within presynaptic terminals, the ER forms a network with a predominantly tubular appearance close to the active zone, which is highly dynamic and undergoes constant movement and reorganization and regularly forms contact sites with the plasma membrane (Wu et al., 2017; Cohen et al., 2018). The dynamic movements of ER are regulated by the cytoskeleton and motor proteins. Live-cell fluorescence microscopy studies have shown that microtubules regulate ER movements in animal cells (Waterman-Storer and Salmon, 1998; Lu et al., 2009; Wozniak et al., 2009; Friedman et al., 2010), whereas in plants (Griffing, 2010) and budding yeast cells (Prinz et al., 2000;

Du et al., 2006) ER movements require actin. Similarly, in neurons, microtubules provide a structural backbone for gross dendritic and axonal ER movements (Farias et al., 2019). Other studies have revealed a specific role of myosin Va (encoded by *Myo5a*) in ER transport along actin filaments into dendritic spines, demonstrating that ER import into these subcellular compartments might be actin dependent (Wagner et al., 2011). Whether similar actin-dependent mechanisms also determine the movement of axonal ER remains unclear. In this study, we show that in axons, the ER appears associated with actin filaments, especially in growth cone filopodia where actin filaments are highly enriched. The importance of the axonal ER dynamic regulation is highlighted by mutations in ER-shaping or ER-receptor proteins that impair ER remodeling and associate with neurodegenerative diseases such as amyotrophic lateral sclerosis (ALS) (Teuling et al., 2007) or hereditary spastic paraplegia (HSP) (Blackstone, 2012; Öztürk et al., 2020).

In neurons, rough cisternal ER (RER) – the major site for protein synthesis, folding, processing and secretion – appears mainly restricted to the somatodendritic compartment (Horton and Ehlers, 2003; Shibata et al., 2010; West et al., 2011; Puhka et al., 2012; Lee et al., 2020). Axons are traditionally considered to be devoid of RER, as demonstrated by ultrastructure electron microscopy studies, and are thought to exhibit only smooth ER (Tsukita and Ishikawa, 1976; Krijnse-Locker et al., 1995). The function of such axonal ER has been suggested to be limited to lipid metabolism, Ca^{2+} homeostasis and to functions in contacting membranous organelles to regulate their biogenesis and maintenance (Tsukita and Ishikawa, 1976; Wu et al., 2017; Farias et al., 2019; Lee et al., 2020). Nevertheless, despite emerging evidence of intra-axonal translation of mRNAs encoding membrane and secreted proteins in isolated neurons (Merianda et al., 2009), there is no direct evidence for the existence of an RER in axons that could process such locally synthesized proteins for integration into the axoplasmic membrane and secretion.

Here, we investigated the interaction of ribosomes with the ER in the axonal growth cones of cultured motoneurons and found that ribosomes undergo rapid changes in distribution and structure in response to extracellular cues. We used culture conditions with human merosin (laminin-221 and laminin-211) that promote differentiation of presynaptic structures in axon terminals (Jablonka et al., 2007). In such differentiated growth cones with presynaptic structures, ribosomes relocate to the ER where they accomplish local translation of membrane-associated and secreted proteins, including TrkB (also known as NTRK2) and N-type Ca^{2+} channels. Furthermore, we unraveled the underlying mechanisms for regulation of ER dynamic movements in axon terminals and showed that fast dynamic elongation of ER into axonal filopodia is regulated mainly by actin and its motor protein myosin VI (encoded by *Myo6*). Conversely, slow ER movements in the growth cone core

depend on a coordinated actin and microtubule cytoskeleton that requires the crosstalk activity of drebrin A. Thus, we provide evidence of a novel function of axonal ER in local protein synthesis of transmembrane proteins, such as the α-1β subunit of presynaptic N-type Ca^{2+} channels (also known as CACNA1B), in addition to its previously described roles.

RESULTS

ER dynamics are regulated by a coordinated actin and microtubule cytoskeleton in growth cones of cultured motoneurons

In axons, membrane-bound organelles representing the ER often colocalize with, and hardly extend beyond, microtubules (Dailey and Bridgman, 1989; Farias et al., 2019). Nevertheless, growth cone filopodia that contain differentiated presynaptic active zone structures (Jablonka et al., 2007) are enriched in actin filaments and mostly lack microtubules (Geraldo and Gordon-Weeks, 2009). Thus, we wondered whether the ER in axonal growth cones could extend into these actin-rich filopodia and associate with actin filaments in addition to microtubules. In order to visualize the ER in growth cones, we transduced primary cultured motoneurons with a lentivirus expressing mCherry–KDEL (referred to hereafter as mCherry–ER), a well-studied ER marker (Guo et al., 2018). Neurons were then fixed and immunostained to visualize F-actin and the microtubule cytoskeleton using phalloidin and α-tubulin staining, respectively. The association of the ER with actin and tubulin in axon terminals was then assessed using structured illumination microscopy (SIM) (Fig. S1). Interestingly, ER was not only detected in the core of growth cones but also in filopodia (Fig. S1A). Three-dimensional (3D) reconstruction and line scan analysis showed that ER colocalizes with both F-actin and microtubules in the core, while in filopodia, the ER overlaps mostly with F-actin, as expected given that microtubules are less abundant in filopodia (Fig. S1B,C). To rule out colocalization by chance, we rotated the ER channel by 90° and could detect only a small overlap between the ER and either F-actin or α-tubulin (Fig. S1D). Next, we performed live-cell imaging over a period of 8 min with 2 s intervals to visualize ER movements in the axonal growth cone. We transduced motoneurons with mCherry–ER lentivirus and co-transduced with a lentivirus expressing a cell volume marker (GFP) for simultaneous visualization of the plasma membrane movements (Fig. 1A; Movie 1). Notably, the ER entered only a fraction of highly dynamic filopodia in axonal growth cones during the time of observation, indicating that ER movement is only partially coupled to movements of the plasma membrane (Fig. 1B). To confirm the colocalization of the ER with F-actin in filopodia, we monitored the dynamics of ER and actin co-movements in filopodia by transducing motoneurons with a GFP-actin-IRES-mCherry-KDEL lentivirus. This lentiviral construct expresses both GFP–actin and mCherry–ER and thus allows visualization of actin and ER movements in the same filopodia simultaneously (Fig. 1C,D). Two-color live-cell imaging demonstrated that in filopodia, tubular ER extends and retracts along actin filaments, indicating that ER interaction with actin defines its rearrangement and remodeling (Movie 2). It is of note that in some filopodia, the ER collapsed while actin filaments remained stable (Movie 3). To quantify ER dynamic movements, we implemented an adaptation of image correlation spectroscopy (ICS) (Wiseman, 2015), which measures the dynamics as intensity movements (μm/sec) (Fig. 1E). ICS analysis revealed distinct motilities for actin and ER in the same filopodia, which excludes the possibility that ER extension and retraction events are forced by actin movements (Fig. 1F). Based on

these observations, we hypothesized that ER extension into filopodia might be actin dependent and not microtubule dependent. To address this, we transduced motoneurons with mCherry–ER and disrupted F-actin or microtubules using the depolymerizing drugs cytochalasin D (CytoD) or nocodazole, respectively. Motoneurons were treated with 1 μg/ml CytoD for 30 min or 10 μM nocodazole for 2 h, and ER movements were then evaluated in the growth cone using live-cell imaging (Fig. 2A,B; Movies 4–9). ICS analysis did not detect any movements in fixed cells, indicating that the error of ICS analysis is very low (Fig. 2C). In addition to ICS analysis, we used multiple kymographs to measure the frequency and distance moved by the ER in the axonal growth cones manually. Intriguingly, we found that dynamic movement of the ER in filopodia was significantly higher than that in the core (Fig. 2C). Furthermore, the velocity of dynamic movements was higher, as represented in Fig. 2D, and the distance moved by the ER in filopodia was greater than the distance moved in the growth cone core, correspondingly (Fig. 2E). Moreover, we found that upon CytoD treatment, 80% of neurons failed to show ER movements in filopodia, whereas only 40% failed to show ER movements in the core (Fig. 2F). Treatment with nocodazole resulted in 50% of neurons failing to show ER movements in filopodia and 40% of neurons failing to show ER movements in the growth cone core (Fig. 2F). ICS analysis revealed that disruption of either actin or microtubule dynamics reduces ER movements significantly in both filopodia and the growth cone core, implying that ER dynamic movements depend on a coordinated actin and microtubule cytoskeleton (Fig. 2G,H). Nevertheless, analyzing the frequency of ER movements in filopodia demonstrated that disruption of actin, but not microtubules, reduced the frequency of ER movements (Fig. 2G). In contrast to filopodia, the frequency of ER movements in the growth cone core was markedly reduced upon disruption of either actin or microtubules, which is in agreement with the above ICS analysis (Fig. 2H). This finding was further confirmed by a treatment with both CytoD and nocodazole, which severely impaired the ER dynamics in both filopodia and the growth cone core, as nearly no ER movements were detectable under this condition (Fig. 2F–H; Fig. S2A).

Collectively, these data provide evidence of a highly dynamic ER in axonal growth cones of developing motoneurons. The dynamic movements of the ER in axonal growth cones could be classified into fast movements in filopodia and slower movements in the core. Fast ER remodeling in filopodia is regulated particularly by the actin cytoskeleton, whereas slow ER rearrangements in the core require microtubule and actin crosstalk.

Myosin VI tethers the ER in axonal filopodia

Next, we asked which myosin motor protein is involved in actin-mediated ER tethering in axonal growth cone filopodia. A previous study has shown that myosin Va translocates the ER into dendritic spines of Purkinje neurons (Wagner et al., 2011). To examine the possible role of different myosin isoforms, we treated motoneurons with pharmacological inhibitors of myosin II [(−)-blebbistatin], myosin V (MyoVin-1) and myosin VI (2,4,6-triiodophenol) and analyzed the ER movements in growth cones using live-cell imaging (Fig. 3A). First, we tested the toxicity of these inhibitors in a survival assay using concentrations ranging between 1 μM and 100 μM and tested incubation times of 30 min up to 12 h. Treatments with 5 μM (−)-blebbistatin, 30 μM MyoVin-1 and 1 μM 2,4,6-triiodophenol for 15 min seemed not to affect the neuronal viability and were therefore chosen for this experiment (Fig. S3A–C). Pharmacological inhibition of myosin V or myosin
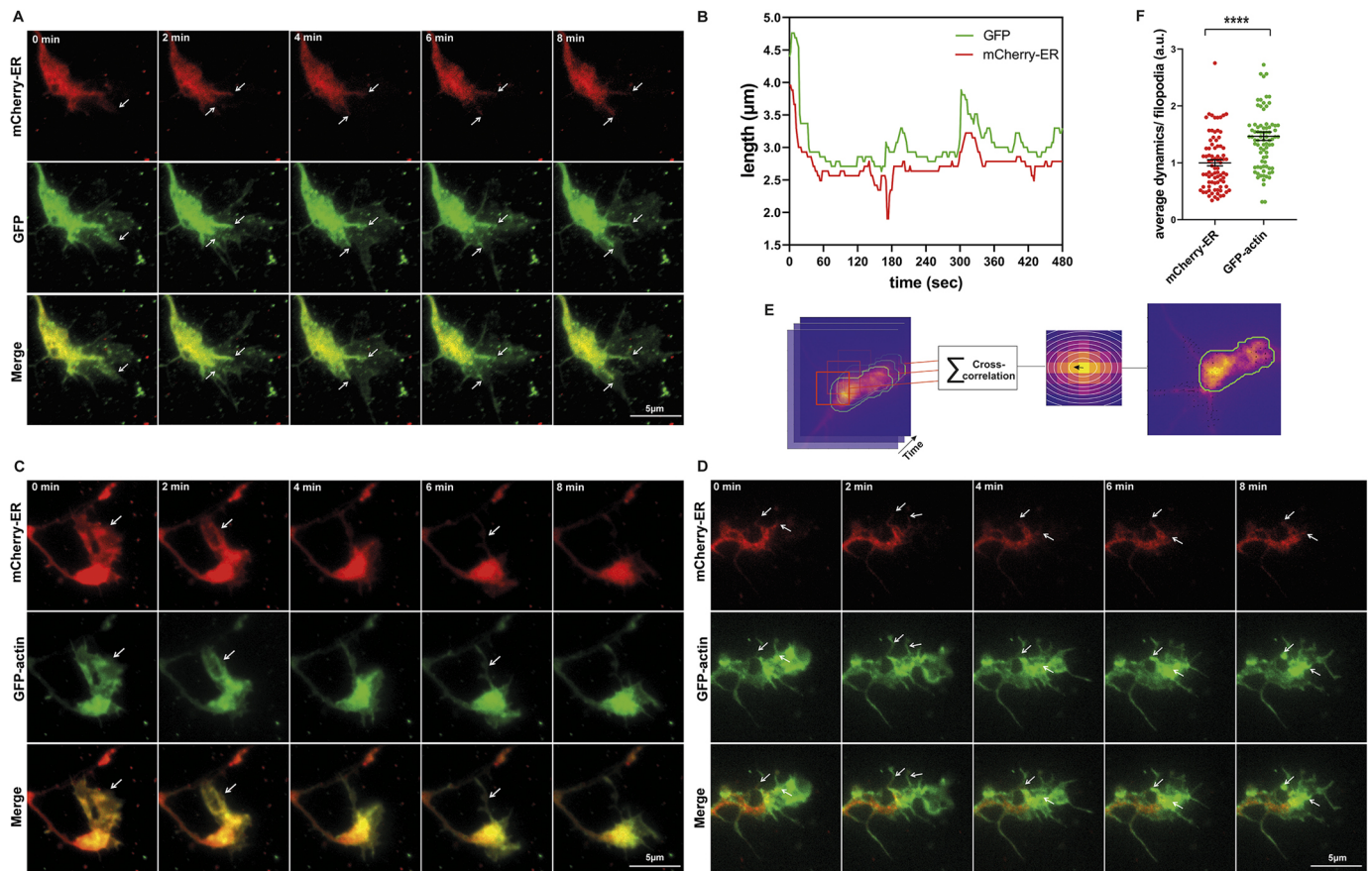
Fig. 1. ER moves along actin filaments in growth cone filopodia. (A) Representative time-lapse images of motoneurons transduced with lentiviruses expressing cell volume marker GFP and mCherry–ER. Arrows indicate ER entry into filopodia that are labeled with GFP. (B) Graph shows representative growth and retraction events of ER and plasma membrane (GFP) in a single filopodium over time. (C,D) Representative time-lapse images of motoneurons transduced with a lentivirus co-expressing GFP–actin and mCherry–ER. (C) Arrows indicate co-movements of mCherry–ER and GFP–actin in some filopodia. (D) Arrows indicate that in some filopodia only ER but not F-actin retracts. Data in A–D are representative of three independent experiments. (E) Diagram showing the workflow of ICS implemented in Python (see Materials and Methods for details). (F) Graph shows average dynamics of ER and F-actin movements per filopodium as assessed using ICS (a.u., arbitrary units). Dynamic movements of F-actin are significantly higher than those of ER in the same filopodia. Scatter dot plot with mean±s.e.m. indicated (n=83 filopodia in three independent experiments). ****P<0.0001 (two-tailed Mann–Whitney test).

VI markedly reduced the dynamic movements of the ER in both the core and filopodia of growth cones, with myosin VI inhibition having the strongest effect, whereas inhibition of myosin II was much less effective (Fig. 3B,C; Movies 10–12). These data indicate that in motoneurons, myosin VI in particular drives ER movements in axonal growth cones.

Drebrin A regulates axonal ER movements via actin and microtubule crosstalk

Previous studies have revealed that drebrin mediates crosslinking between actin and microtubules through direct interaction with actin filaments and the microtubule end-binding protein 3 (EB3, also known as MAPRE3) (Geraldo et al., 2008; Worth et al., 2013). This drebrin-dependent actin–microtubule crosstalk is required for neuronal migration (Trivedi et al., 2017) and neuritogenesis (Geraldo et al., 2008). Thus, we sought to examine whether the coordination between actin and microtubules that is required for ER movements in axonal growth cones depends on drebrin. Drebrin has two major isoforms; neuronal-specific drebrin A, which is highly expressed in the adult brain, and embryonic isoform drebrin E, which is also expressed in non-neuronal cells (Shirao et al., 2017). We found similar expression levels of these two isoforms in our

cultured motoneurons from mouse embryos. To examine the role of these isoforms in axonal ER movements, we designed two different lentiviral shRNAs that target either drebrin A (shDrebrin A) or both drebrin A and E (shDrebrin A+E). These lentiviral constructs co-expressed GFP, which was used to identify transduced cells. As control, we used the empty shRNA vector backbone expressing only GFP (shCtrl). A reverse transcription-quantitative PCR (qRT-PCR) assay showed that transduction of motoneurons with shDrebrin A leads to 90% reduction in drebrin A mRNA levels and that transduction with shDrebrin A+E results in 90% reduction in drebrin A and 94% reduction in drebrin E mRNA levels (Fig. 4A). Next, we co-transduced motoneurons with mCherry–ER and either shDrebrin A, shDrebrin A+E, or shCtrl, and analyzed the ER dynamic movements in axonal growth cones using live-cell imaging (Fig. 4B; Movies 13,14). We found that knockdown of drebrin A decreased ER dynamic movements by 40% in filopodia (Fig. 4C) and by 30% in the growth cone core (Fig. 4D). As illustrated in Fig. 4C,D, additional knockdown of drebrin E did not further decrease the ER movements, indicating that drebrin A, but not drebrin E, is relevant for coordinating actin and microtubule functions involved in ER movements in the axonal growth cone.
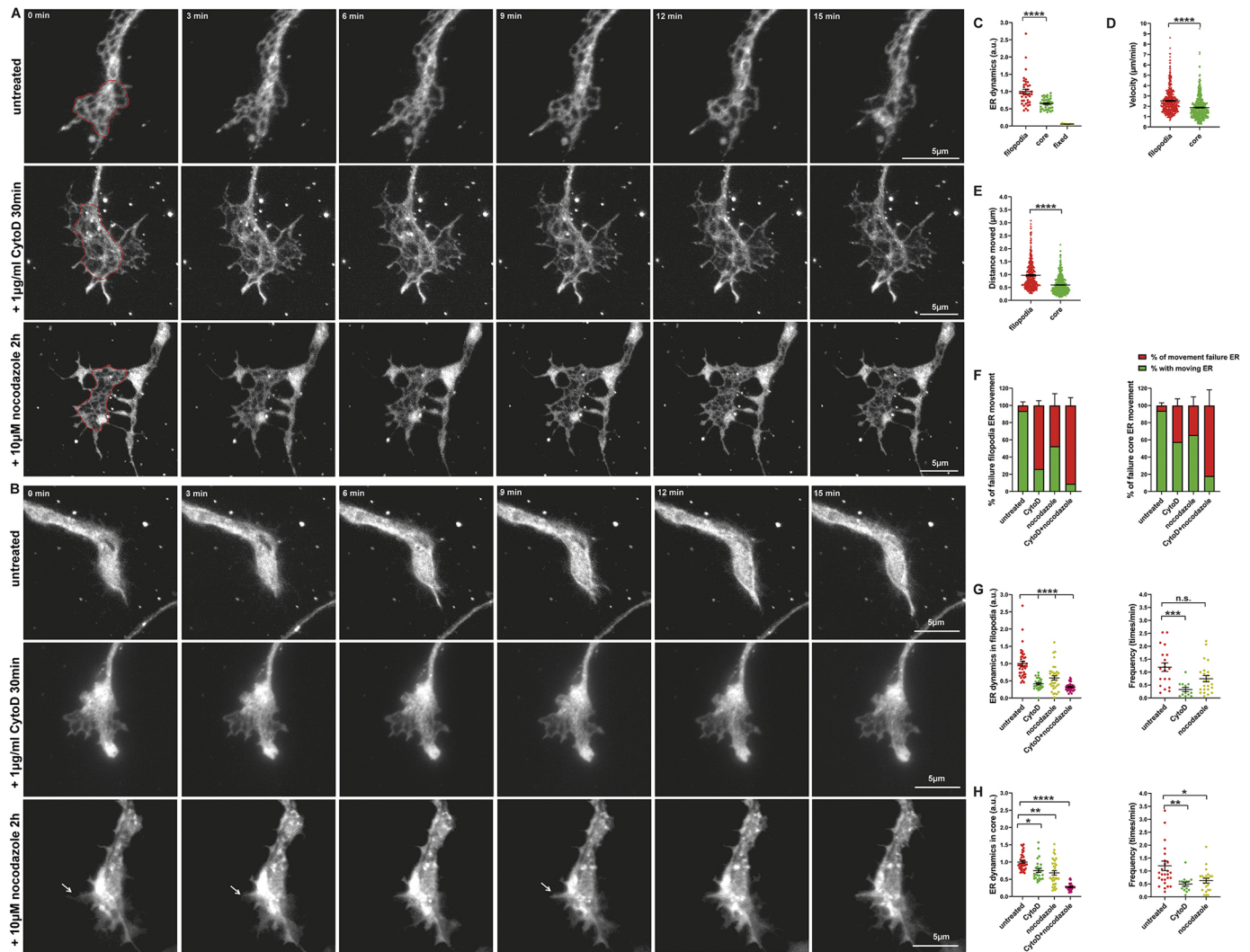
Fig. 2. ER dynamic movements are regulated by actin and microtubules in the growth cone core and filopodia. (A,B) Representative time-lapse images of motoneurons expressing mCherry–ER in the growth cone core (A) and filopodia (B) in the presence or absence of the indicated CytoD and nocodazole treatments. Growth cone cores are outlined in red, and arrows show ER extension into filopodia. (C) Graph shows ICS analysis of ER movements in filopodia and in the growth cone core (a.u., arbitrary units). Analysis of fixed motoneurons is shown as a control. ER dynamic movements are higher in filopodia than in the core. $n=40$ cells from six independent experiments. ****$P<0.0001$. (D,E) Kymograph analysis of velocity of ER movements (D) and distance moved by the ER (E) in filopodia and in the growth cone core. $n=25–29$ cells from three independent experiments. ****$P<0.0001$. (F) Average percentage of neurons failing to show ER movements in filopodia (left panel) or the growth cone core (right panel) upon the indicated treatments ($n=32–55$ cells from three independent experiments). (G) Average ER movements (left panel, $n=27–40$ cells from four or five independent experiments) and frequency of ER movements (right panel, $n=12–23$ from three to five experiments) in filopodia per growth cone. In filopodia, the frequency of ER movements is decreased upon CytoD treatment (***$P=0.0004$; $n=12–20$ cells from four or five experiments), but not nocodazole treatment (n.s., $P=0.1079$; $n=20–23$ cells from four or five independent experiments). Combined CytoD and nocodazole (CytoD+nocodazole) treatment decreases ER movements in filopodia (****$P<0.0001$; $n=28–40$ cells from three independent experiments). (H) Average ER movements (left panel; *$P=0.0353$; **$P=0.0012$; $n=27–40$ cells from four or five independent experiments) and frequency of ER movements (right panel; **$P=0.0016$; *$P=0.0271$; $n=15–27$ cells from four to six independent experiments) in the core per growth cone. CytoD+nocodazole treatment decreases core ER movements (****$P<0.0001$; $n=28–40$ cells from three independent experiments). Data are presented as bar diagrams or scatter dot plots with mean±s.e.m. indicated. Statistical analyses used a one-way ANOVA with Dunn's post-hoc test in G and H, and a two-tailed Mann–Whitney test in C–E.

Extracellular stimulation triggers ribosome activation and initiates local translation in growth cones on a time scale of seconds

Deep RNA-seq combined with sensitive fluorescence *in situ* hybridization (FISH) approaches have identified numerous mRNAs (Briese et al., 2016; Holt et al., 2019) within distal axons which are locally translated (Moradi et al., 2017; Terenzio et al., 2018; Biever et al., 2020). Locally synthesized proteins are necessary for neural circuit development, survival and plasticity (Fernandopulle et al., 2021). In developing axons, local translation mediates an essential response to guidance cues required for

pathfinding (Leung et al., 2006). Brain-derived neurotrophic factor (BDNF) and its receptor TrkB play a vital role in modulation of local translation (Santos et al., 2010) and axonal cytoskeleton remodeling (Sasaki et al., 2010; Rathod et al., 2012) in motoneurons. We sought to scrutinize the dynamics of ribosome activation in response to BDNF stimulation in the growth cone of motoneurons. Following BDNF binding, TrkB undergoes autophosphorylation and activates mitogen-activated protein kinase (MAPK) as well as phosphoinositide 3-kinase (PI3K)–AKT signaling pathways (Huang and Reichardt, 2003; Hua et al., 2016), leading to activation of ribosomes and induction of local translation (Leal
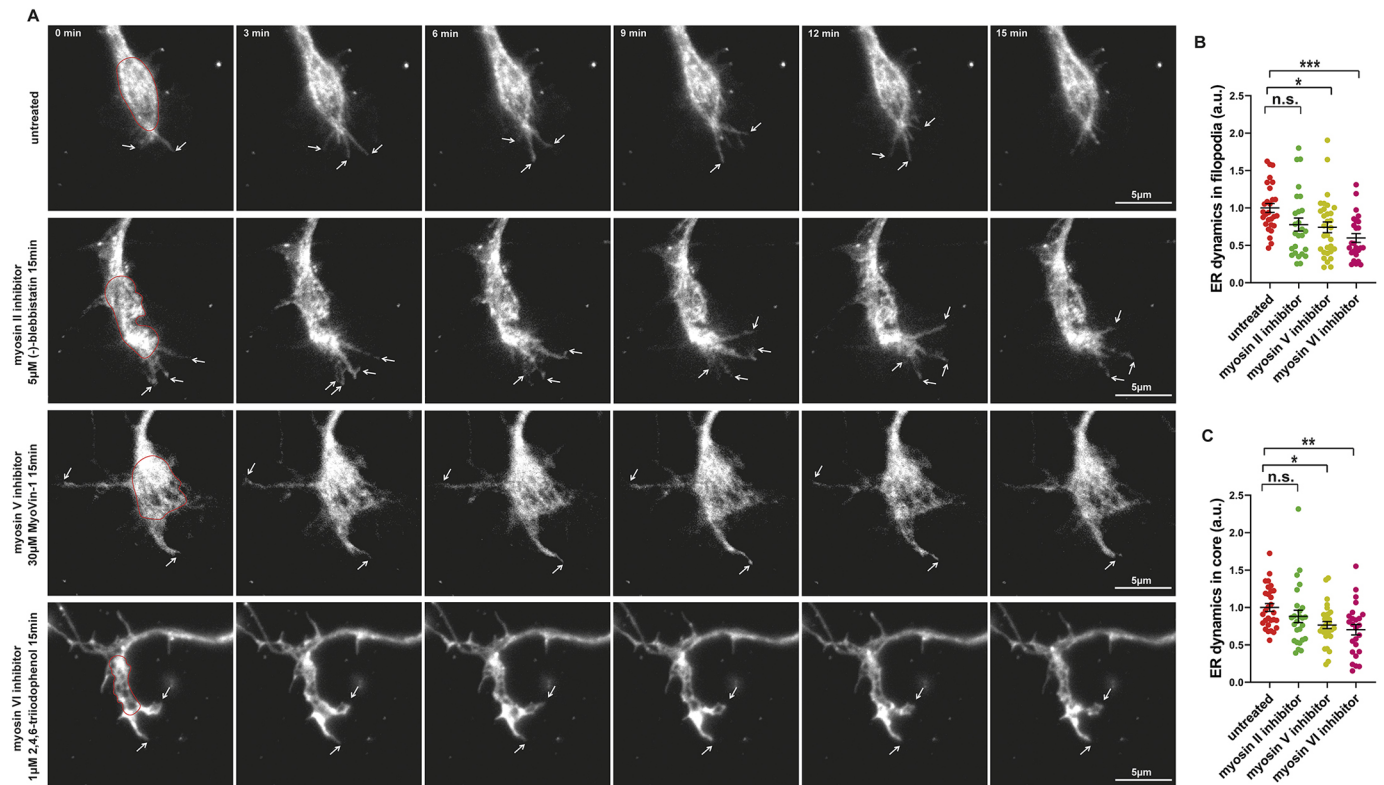
Fig. 3. ER entry into axonal growth cone filopodia depends on myosin VI. (A) Representative time-lapse images of the ER in growth cones of motoneurons treated with myosin II, V or VI inhibitors and of untreated control motoneurons. ER in growth cone cores is outlined in red, and white arrows indicate the movements of filopodial ER. (B) Quantification of ER dynamics in mCherry–ER-transduced motoneurons reveals significant reduction in ER movements in axonal filopodia upon inhibition of myosin V (*$P<0.0361$) and VI (***$P<0.0005$). $n=26–31$ cells from four independent experiments. (C) Graph shows reduced ER dynamic movements in the growth cone core after treatments with myosin V (*$P<0.0339$) and myosin VI inhibitors (**$P<0.0099$). $n=26–31$ cells from four independent experiments. Data are presented as scatter dot plots with mean±s.e.m. indicated (a.u., arbitrary units; n.s., not significant). Statistical analyses used a one-way ANOVA with Dunn's post-hoc test.

et al., 2014). In order to define the precise kinetics of TrkB activation, we applied BDNF to motoneurons with a short pulse of 10 s, 1 min or 10 min, then washed out the BDNF and immunostained neurons to label TrkB and phosphorylated TrkB (pTrkB). The specificity of TrkB and pTrkB antibodies was confirmed by immunostaining using TrkB-knockout mice (Fig. S4A,B). We could detect pTrkB upon 10 s BDNF pulse in the growth cone, as shown by our immunofluorescence assay (Fig. 5A,B). Interestingly, the levels of TrkB were also elevated in the growth cone after 1 min BDNF exposure (Fig. 5C). In the whole-cell lysate, a corresponding elevation of pTrkB immunoreactivity first became detectable at 1 min post stimulation, as shown by western blotting (Fig. 5D), and no increase in total level of TrkB was detectable after 10 min stimulation, indicating that this short pulse is insufficient to induce the transcription and translation of TrkB in the soma (Fig. 5D; Fig. S4C). The rapid increase in TrkB immunoreactivity within less than 1 min of stimulation in the growth cone of motoneurons could be explained by release of this receptor from intracellular stores or changes in the receptor conformation that favor antibody binding. The increase in TrkB immunoreactivity in growth cones observed at the later time point of 10 min post stimulation (Fig. 5C) could be explained by enhanced transport of TrkB from distal axons into growth cones and/or rapid neosynthesis in growth cones, since TrkB mRNAs were detected in axons by qRT-PCR assay (Fig. S4D). Treatment of neurons with either 100 ng/ml anisomycin for 1 h, which inhibits translation, or 10 μM nocodazole for 2 h, which blocks microtubule-based

transport, prevented the increase in TrkB signal in growth cones (Fig. 5E,F). These data indicate that BDNF stimulation triggers redistribution of TrkB, resulting in an increase in TrkB total immunofluorescence within 1 min, and also induces its local production within 10 min stimulation.

In developing axons, the rapid response to extracellular cues is assured by tight regulation of spatiotemporal changes in mRNA translation (Willis et al., 2007; Yoon et al., 2009). Thus, the kinetics of induction of ribosomal changes that trigger translation in growth cones should differ from those in the soma. To study the dynamics of ribosome remodeling, we used binding of the anti-rRNA antibody Y10B as a general marker for ribosomes and RPL8 as a marker for the 60S ribosomal subunit in order to study the dynamics of movement of these different ribosomal components. We found that induction of BDNF–TrkB signaling led to a rapid change in the distribution of these ribosomal markers within the growth cone. The immunoreactivities of ribosomal markers Y10B epitope and RPL8 were rapidly altered and appeared increased after 10 s BDNF pulse (Fig. 5G–I). Interestingly, short BDNF pulses of 10 s and 1 min were not sufficient to induce such changes in ribosome distribution in the soma, as shown in Fig. S4E, despite TrkB phosphorylation being detected in this subcellular compartment after 10 s stimulation (Fig. S4F). This kinetic distinction suggests that in the growth cone, BDNF–TrkB signaling and downstream mechanisms for modulating ribosome distribution and possibly also ribosome activation are different from those in cell bodies. Increased immunoreactivity for ribosomal subunits in the growth cone
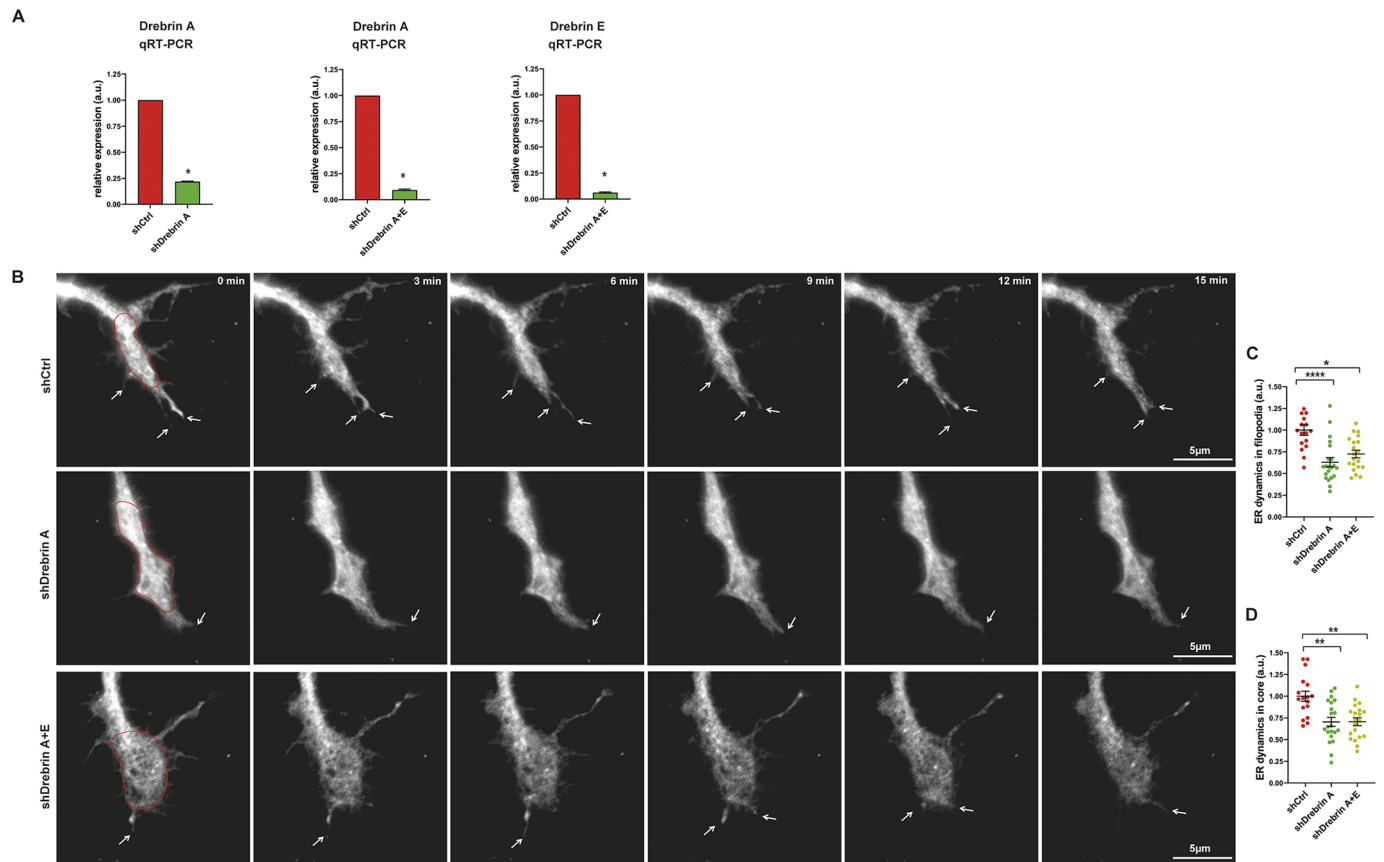
Fig. 4. Drebrin A mediates actin- and microtubule-coordinated ER movements in axonal growth cones. (A) Graphs show relative mRNA expression of drebrin A and drebrin E in motoneurons transduced with shDrebrin A or shDrebrin A+E. shRNA-mediated knockdown of drebrin A results in 80% reduction in drebrin A mRNA levels (left panel). shRNA targeting both drebrin A and drebrin E (shDrebrin A+E) causes 90% reduction in drebrin A mRNA levels (middle panel) and 94% reduction in drebrin E mRNA levels (right panel). *$P<0.05$; from three independent experiments. (B) Representative time-lapse images of ER in motoneuron growth cones transduced with shDrebrin A, shDrebrin A+E or shCtrl lentiviruses, as indicated. ER in the growth cone core is outlined in red, and ER movements in filopodia are indicated by white arrows. (C) Graph shows dynamics of ER movements in axonal growth cone filopodia. Knockdown of drebrin A significantly reduces the ER movements in filopodia (****$P<0.0001$). Knockdown of drebrin E in addition to drebrin A does not further reduce the ER movements in filopodia (*$P=0.0133$). $n=17$–21 cells from three independent experiments. (D) ER movements in the growth cone core are depicted. Knockdown of drebrin A causes significant reduction in ER movements in the growth cone core (**$P=0.0026$), whereas additional knockdown of drebrin E does not intensify this effect (**$P=0.0019$). $n=17$–21 cells from three independent experiments. Data are presented as bar diagrams or scatter dot plots with mean±s.e.m. indicated (a.u., arbitrary units). Statistical analyses used a one-tailed Mann–Whitney test in A and one-way ANOVA with Dunn's post-hoc test in C and D.

within 10 s BDNF stimulation is striking. Rapid transport of ribosomal subunits from axonal sites to the growth cone appears unlikely since the fastest measured microtubule-dependent axonal transport at a speed of 4.6 µm/s cannot provide ribosomes from the axon shaft into growth cones within such a short time (Maday et al., 2014; Wortman et al., 2014). To exclude this possibility, we treated neurons with nocodazole to disrupt microtubule-based axonal transport and found that disruption of axonal transport did not affect BDNF-induced augmentation of ribosomal subunits, as illustrated in Fig. 5J. Similarly, inhibition of translation by anisomycin treatment resulted in a significant increase in ribosome immunoreactivity, indicating that this increase does not depend on *de novo* synthesis of ribosomal proteins within the growth cone (Fig. 5K). Strikingly, treatment with 1 µg/ml CytoD for 30 min completely prevented the ribosomal response to BDNF stimulation, as no increases in the signal intensities of Y10B epitope and RPL8 were detectable upon either stimulation interval (Fig. 5L,M). Based on these observations, we propose that elevated immunoreactivity of ribosomes within 10 s stimulation might be due to actin-dependent conformational and distribution changes in ribosomal subunits that occurs upon assembly of 80S subunits and thus alters

accessibility of the epitopes that are detected by the Y10B and RPL8 antibodies. To investigate this hypothesis, we stained motoneurons with antibodies against RPL24 of the 60S and RPS6 of the 40S subunits (Fig. 6A). Upon assembly of 80S ribosomes, the C terminus of RPL24 interacts with RPS6, thereby forming a bridge between the two subunits (Ben-Shem et al., 2011). We employed SIM with a resolution of ~120 nm to examine the interaction of RPL24 with RPS6 in growth cones. As depicted in Fig. 6B, within 10 s of BDNF stimulation the occurrence of co-clusters of RPL24 and RPS6 increased by threefold compared to the no stimulation condition. Similarly, colocalization of RPL24 and RPS6 increased significantly at 10 s and 1 min post stimulation (Fig. 6C). Thus, we reasoned that the rapid increase in immunoreactivity of Y10B epitope in response to extracellular stimulation involves extremely fast assembly of ribosomes into 80S subunits. Strikingly, 80S subunits seem to disassemble after a long stimulation of 30 min, as the number of RPL24–RPS6 co-clusters as well as their colocalization declined. This observation implies a rapid but transient response of ribosomes to extracellular stimuli (Fig. 6B,C). Strikingly, inhibition of actin polymerization via CytoD treatment impeded the formation of RPL24–RPS6 co-clusters (Fig. 6D).
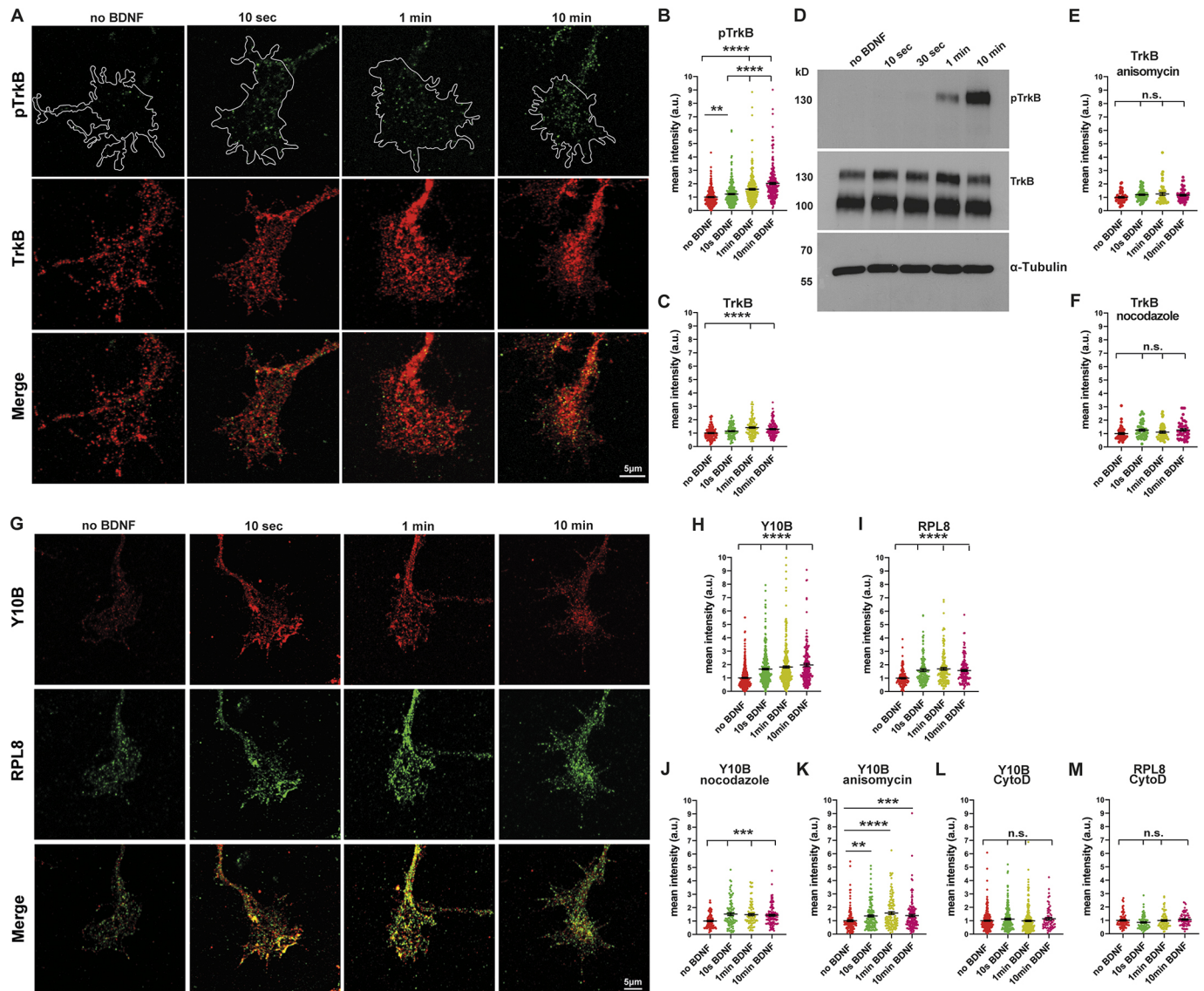
Fig. 5. BDNF-induced TrkB activation triggers redistribution of ribosomes in growth cones. (A) Representative images of growth cones of motoneurons stimulated with BDNF for the indicated times and stained for pTrkB and TrkB. White outlines indicate analyzed regions of interest within the growth cones. (B,C) Mean intensities of pTrkB increase at 10 s (**P=0.0063; n=265–267 cells) and mean intensities of pTrkB and TrkB increase at 1 min (****P<0.0001; n=123–274 cells) and 10 min post stimulation with BDNF (****P<0.0001; n=120–266 cells). Cells analyzed for pTrkB and TrkB intensities were from eight and four independent experiments, respectively. (D) Representative immunoblot of total lysates from cultured motoneurons probed for pTrkB, TrkB and α-tubulin. Duration of BDNF treatments are indicated. Blots are representative of a single experiment. (E,F) Total levels of TrkB in BDNF-stimulated growth cones treated with (E) anisomycin (n.s., P≥0.0893; n=47–54 cells from two independent experiments) or (F) nocodazole (n.s., P≥0.1526; n=45–46 cells from two independent experiments). (G) Representative images of BDNF-stimulated growth cones stained using Y10B and anti-RPL8 antibodies. (H,I) Mean intensities of (H) Y10B and (I) RPL8 signals increase at 10 s (****P<0.0001; n=138–366 cells from nine and four independent experiments for Y10B and RPL8, respectively), 1 min (****P<0.0001; n=138–366 cells from nine and four independent experiments for Y10B and RPL8, respectively) and 10 min post BDNF stimulation (****P<0.0001; n=138–210 cells from six and four independent experiments for Y10B and RPL8, respectively). (J,K) Y10B immunoreactivity increases despite (J) nocodazole (***P≤0.0004; n=93–102 cells from three independent experiments) or (K) anisomycin treatment (**P=0.0012; ***P=0.0008; ****P<0.0001; n=121–141 cells from five independent experiments). (L,M) Upon CytoD treatment, (L) Y10B (n.s., P≥0.5207; n=68–252 cells from three to six independent experiments) and (M) RPL8 immunoreactivities (n.s., P≥0.2256; n=68–87 cells from three independent experiments) do not increase following BDNF stimulation. All data are normalized to the average intensities of the no BDNF group and are presented as scatter dot plots with mean±s.e.m. indicated (a.u., arbitrary units). Statistical analyses used a one-way ANOVA with Dunn's post-hoc test.

Consistent with the data represented in Fig. 5L,M, these data clearly show that ribosome distribution and assembly depend on the actin cytoskeleton. The increased interaction of RPL24 and RPS6 ribosomal proteins and, consequently, the assembly of 80S ribosomes suggest that this conformational change could correlate with translation initiation. To visualize actively translating ribosomes, we co-stained motoneurons to detect the Y10B

epitope, as a structural component of ribosomes, and the elongation factor eEF2, which only associates with actively translating ribosomes (Fig. 6E). Again, we found a significant increase in the number of Y10B and eEF2 co-clusters within 10 s of stimulation, indicating that the response of ribosomes in growth cones to activation of TrkB receptors is very fast (Fig. 6F). Colocalization analysis confirmed increased association of eEF2
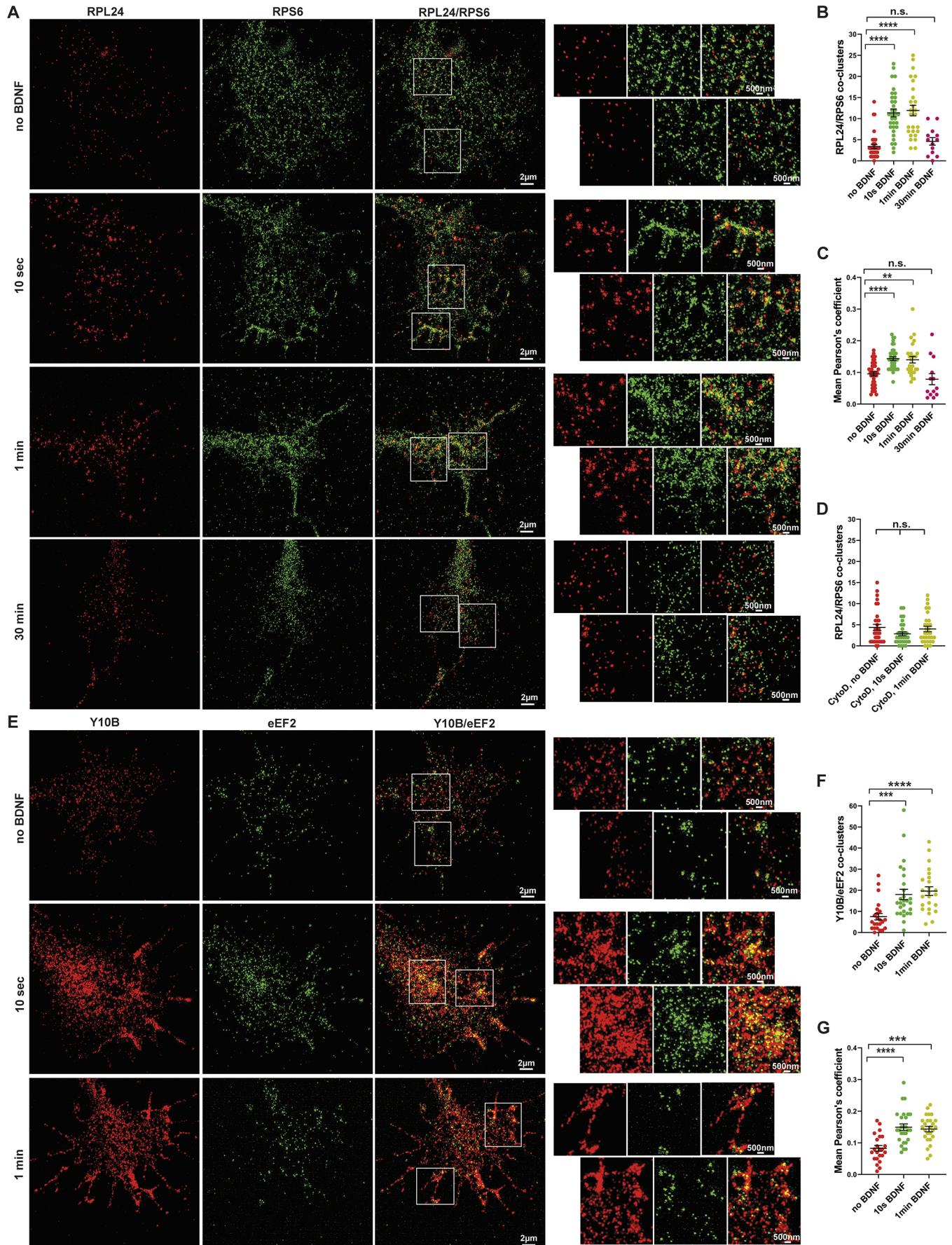
Fig. 6. See next page for legend.

Fig. 6. BDNF stimulation induces ribosomal assembly and initiates translation in growth cones of motoneurons. (A) Representative SIM images of growth cones of BDNF-stimulated wild-type motoneurons stained for RPL24 and RPS6. White squares indicate regions of interest (ROIs) shown in magnified growth cone images on the right. (B) Quantification of RPL24 and RPS6 co-clusters that are representative of fully assembled 80S subunits shows that BDNF stimulation induces formation of RPL24 and RPS6 co-clusters at 10 s and 1 min (****P<0.0001; n=27–33 cells from three independent experiments), which dissociate again after a long stimulation of 30 min (n.s., P>0.99; n=13 from two independent experiments). (C) Pearson's correlation coefficient analysis shows increased colocalization of RPL24 and RPS6 at 10 s and 1 min (****P<0.0001; **P=0.0079; n=26–36 cells from three independent experiments) but not 30 min (n.s., P>0.99; n=13 from two independent experiments) post stimulation with BDNF. (D) Quantification shows that CytoD treatment affects the BDNF-induced formation of RPL24–RPS6 co-clusters (n.s., P=0.616; n=30–32 cells from three independent experiments). (E) Representative SIM images of growth cones of BDNF-stimulated motoneurons stained using Y10B and anti-eEF2 antibodies. White squares indicate ROIs shown in magnified growth cone images on the right. BDNF stimulation induces formation of Y10B and eEF2 co-clusters at 10 s as well as 1 min. (F) Quantification of Y10B and eEF2 co-clusters that are representative of ribosomes in the elongation phase of translation (***P=0.0007; ****P<0.0001; n=23–27 cells from three independent experiments). (G) Mean Pearson's correlation coefficient shows increased colocalization of Y10B and eEF2 at 10 s and 1 min post stimulation with BDNF (****P<0.0001; ***P=0.0001; n=23–27 cells from three independent experiments). Data are presented as scatter dot plots with mean±s.e.m. indicated. Statistical analyses used one-way ANOVA with Dunn's post-hoc test.

with Y10B signal at 10 s and 1 min stimulations (Fig. 6G). To confirm that the rapid activation of ribosomes depends on BDNF–TrkB signaling, we stained motoneurons from TrkB-knockout mice using Y10B and found that in TrkB-knockout motoneurons, ribosomes failed to respond to 10 s BDNF stimulation (Fig. S4G, H). Next, we questioned whether this rapid activation of ribosomes in response to extracellular stimuli associates with a temporal change in protein synthesis in axonal growth cones. To examine the dynamics of local translation, we applied a time series after BDNF pulse to motoneurons, fixed them and stained against β-actin (Fig. 7A). Remarkably, we observed a significant increase in β-actin signal intensity within 1 min of stimulation suggesting that either the velocity of protein synthesis is extremely high in growth cones or that actin undergoes conformational changes in such a way that this leads to enhanced immunoreactivity (Fig. 7B). To distinguish between these two possibilities and to confirm that elevated levels of β-actin rely on protein synthesis and not transport from the axon, we pretreated neurons with anisomycin and nocodazole as described above and applied BDNF pulses for 10 s to 10 min. Inhibition of protein synthesis prevented the increase of β-actin protein levels, while disruption of microtubule-dependent axonal transport had no influence (Fig. 7C,D). Next, we considered the dynamic local translation of transmembrane proteins such as N-type Ca^{2+} channels (Cav2.2), whose mRNAs localize to distal axons in cultured motoneurons (Briese et al., 2016). Using an antibody against the α-1β subunit of N-type Ca^{2+} channels, we detected increased levels of α-1β subunits within 1 min stimulation in axonal growth cones (Fig. 7E,F). Treatment of the cells with anisomycin diminished this enhancement (Fig. 7G), whereas treatment with nocodazole still resulted in elevated levels of α-1β subunits within 1 min in response to BDNF (Fig. 7H). In addition, we incubated cells with 10 μg/ml puromycin for 10 min to confirm our results (Fig. 7I,J). Similar to β-actin and α-1β subunits of the N-type Ca^{2+} channels, within 1 min of stimulation, synthesis of *de novo* proteins was accomplished, as detected by a marked increase in puromycin immunoreactivity,

supporting the observation of an extremely fast rate of local translation in growth cones (Fig. 7K). In contrast, 1 min and 10 min BDNF stimulations did not trigger translation as measured by puromycin intensity in the soma under the same conditions, again pointing towards different translation kinetics in these distinct compartments (Fig. S4I). In line with this, inhibiting translation but not axonal transport prohibited elevated protein synthesis in response to extracellular stimuli as demonstrated by the puromycin assay (Fig. 7L,M). Taken together, these data indicate that in axon terminals, BDNF–TrkB signaling activates the translational machinery within seconds and thus regulates local protein synthesis at an extraordinarily high speed.

RER is present in the axonal growth cone and contributes to BDNF-induced protein translation

Transcripts encoding membrane and secreted proteins as well as ER resident proteins have been reported to be present in axons, and the corresponding proteins are synthesized and delivered into the axoplasmic membrane (Willis et al., 2005, 2007; Tsai et al., 2006). Initial ultrastructural approaches have identified RER in dendrites (Farah et al., 2005) but only smooth ER in axons (Tsukita and Ishikawa, 1976). However, fluorescence microscopy approaches have identified ER-associated proteins implicated in protein translocation, folding and post-translational modifications as well as proteins of the Golgi apparatus in distal axons, suggesting that axons might contain RER (Merianda et al., 2009). Our data show that transmembrane proteins such as TrkB as well as N-type Ca^{2+} channels undergo intra-axonal translation in response to BDNF stimulation. Accordingly, we considered whether axonal growth cones harbor RER, thereby participating in processing of these locally produced membrane and secretory proteins. To address this hypothesis, we transduced motoneurons with lentiviruses encoding the ER marker mCherry–ER and co-stained against RPL24 and RPS6 as markers of entirely assembled 80S ribosomes (Fig. 8A). In contrast to unstimulated neurons, a significant number of RPL24–RPS6 co-clusters colocalized with ER in axonal growth cones of stimulated neurons, and this colocalization increased after 10 s and 1 min stimulations but dropped again after 30 min BDNF pulse (Fig. 8B). Next, we investigated the role of actin in dynamic assembly of the RER in axon terminals. Interestingly, in line with our previous data shown in Figs 5L,M and 6D, CytoD treatment diminished the translocation of ribosomes toward the ER, confirming the role of actin in the rapid assembly of RER (Fig. 8C). Finally, we examined the attachment of actively translating ribosomes to the ER in axonal growth cones by staining mCherry–ER-expressing neurons using Y10B and eEF2 antibodies, as depicted in Fig. 8D. Similarly, 10 s and 1 min BDNF stimulations caused an increase in colocalization of Y10B and eEF2 co-clusters with the ER, indicating that ribosomes in the elongation stage of translation attach to the ER in axonal growth cones (Fig. 8E). These findings imply that RER exists in the growth cone of developing neurons and thus support a role for the ER in processing and surface delivery of axonally synthesized membrane and secretory proteins.

DISCUSSION

In neurons, the ER forms a highly dynamic network in dendrites and axons. The regulation of axonal ER dynamic movements as well as its function in development and maintenance of synapses have gained emerging interest (Summerville et al., 2016; De Gregorio et al., 2017; Lindhout et al., 2019). In this study, we developed a technique to visualize and quantify the dynamic movements of the ER in axon terminals of cultured motoneurons and used this to show
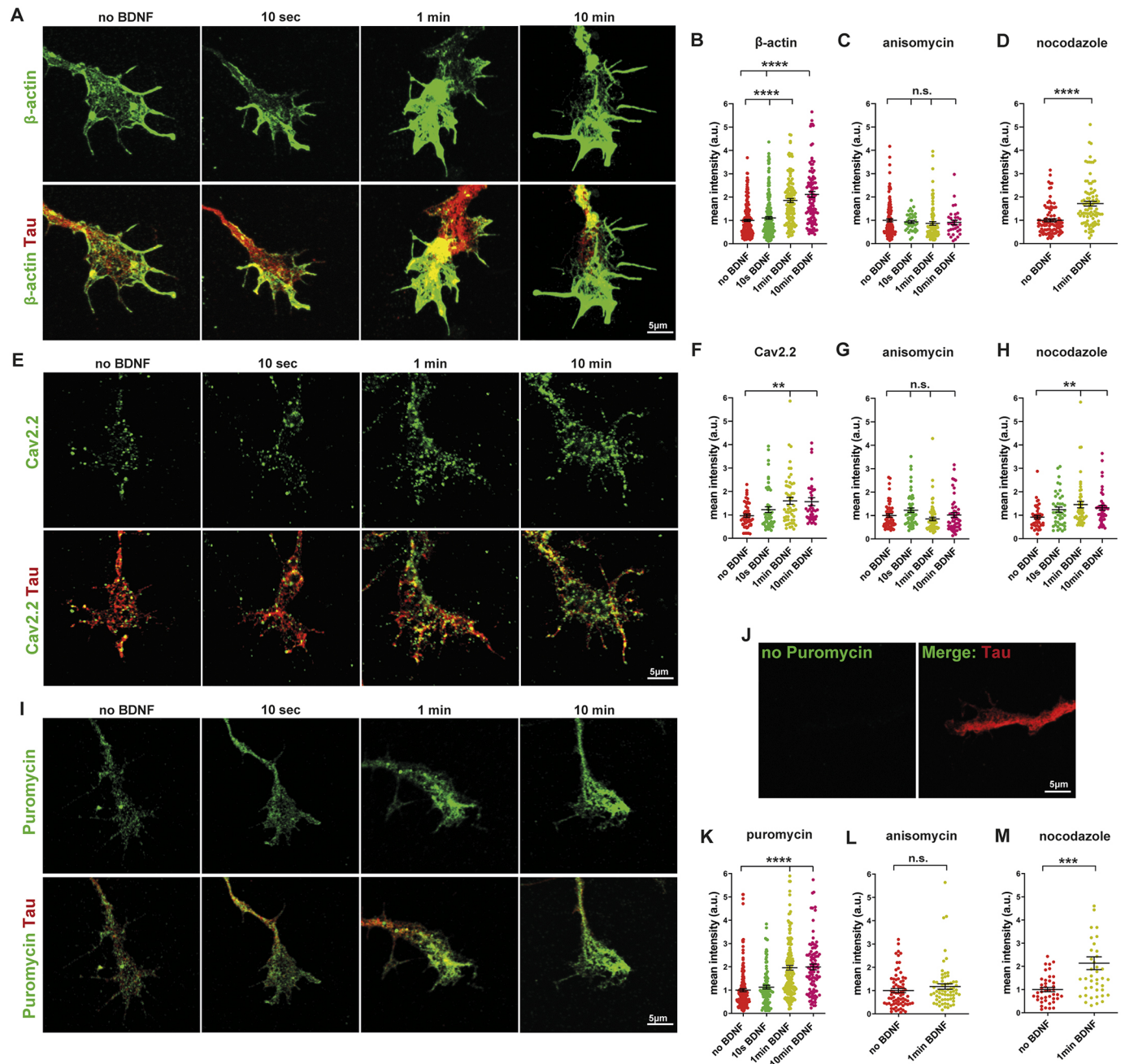
Fig. 7. Rapid effect of BDNF stimulation on protein synthesis in motoneuron growth cones. (A) Representative confocal images of growth cones of BDNF-stimulated motoneurons stained for β-actin (green) and tau (red). (B) Graph shows mean intensities of β-actin in growth cones. A substantial enhancement in mean intensity of β-actin immunoreactivity is first detected after 1 min or 10 min stimulation with BDNF (****P<0.0001; n=114–202 cells from four independent experiments). (C) Anisomycin-treated cells do not show increased levels of β-actin in the growth cone in response to BDNF stimulation (n.s., P≥0.2903; n=33–127 cells from two or three independent experiments). (D) BDNF stimulation for 1 min leads to an increase in β-actin protein levels in nocodazole-treated cells (****P<0.0001; n=91–95 cells from three independent experiments). (E) Representative confocal images of growth cones of BDNF-stimulated motoneurons stained for N-type Ca^{2+} channels (Cav2.2; green) and tau (red). (F) Mean intensities of Cav2.2 increase significantly at 1 min (**P<0.0057) as well as 10 min (**P<0.0085) post stimulation with BDNF. n=50–54 cells from three independent experiments. (G) Anisomycin treatment abolishes the effect of BDNF on Cav2.2 levels in the growth cone (n.s., P=0.26; n=53–67 cells from three independent experiments). (H) Mean intensities of Cav2.2 increase significantly after 1 min (**P<0.0035) and 10 min (**P<0.0099) BDNF pulses in growth cones of nocodazole-treated cells. n=43–50 cells from three independent experiments. (I) Representative confocal images of growth cones of BDNF-stimulated motoneurons treated with puromycin and stained for puromycin (green) and tau (red). (J) As control, puromycin treatment was omitted, and cells were incubated only with primary and secondary antibodies against puromycin and tau. (K) Puromycin immunoreactivity levels are increased at 1 min and 10 min post stimulation with BDNF (****P<0.0001; n=103–218 cells from three to six independent experiments). (L,M) Treatment with (L) anisomycin (n.s., P=0.1796; n=65–73 cells from two independent experiments) but not treatment with (M) nocodazole (***P=0.0002; n=42 cells from two independent experiments) inhibits puromycin immunoreactivity after BDNF stimulation. All data in B–H and K–M are normalized to the average intensities of the no BDNF group. Data are presented as scatter dot plots with mean±s.e.m. indicated (a.u., arbitrary units). Statistical analyses used one-way ANOVA with Dunn's post-hoc test in B,C,F–H and K, and a two-tailed Mann–Whitney test in D,L,M.
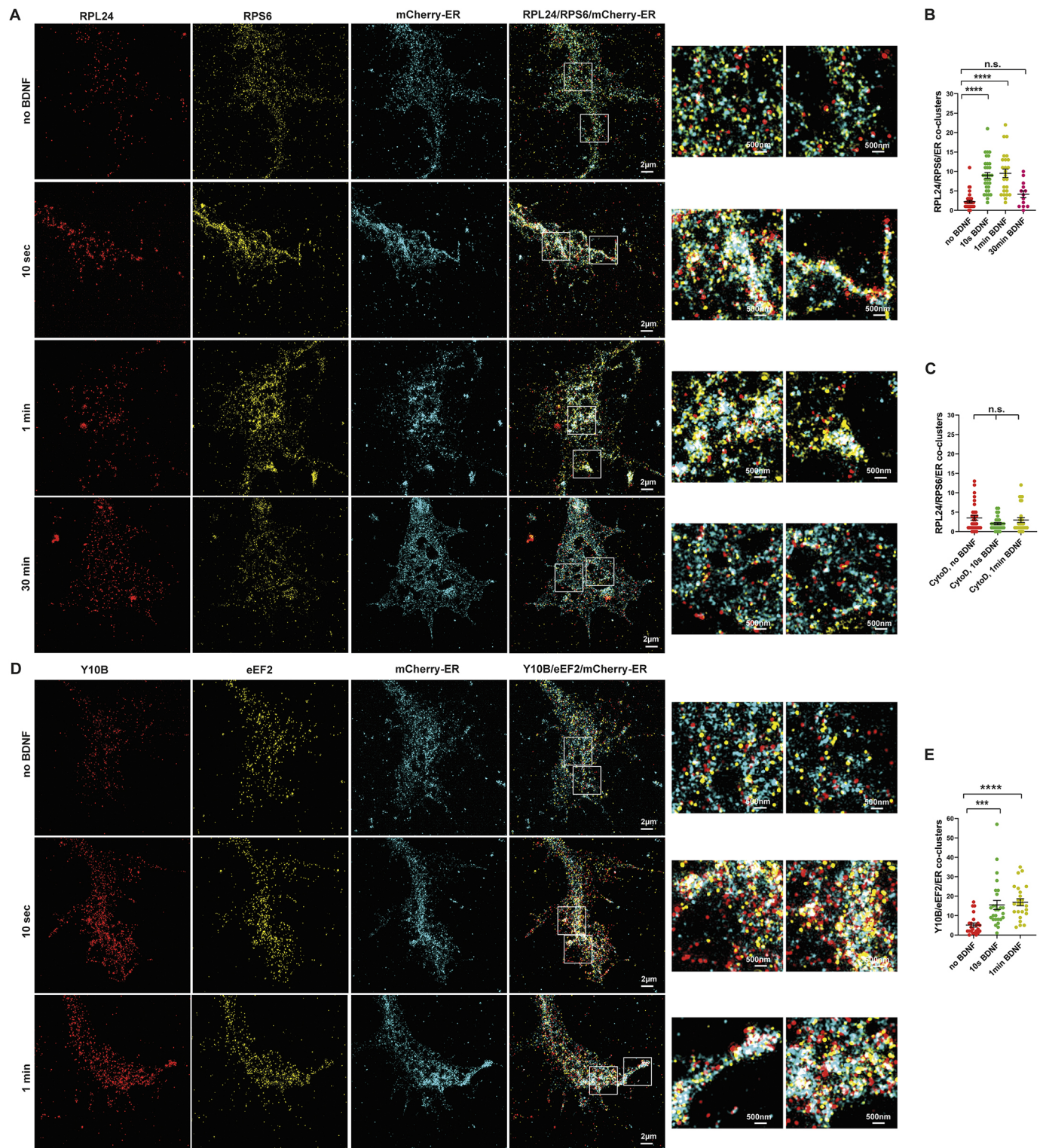
Fig. 8. Ribosomes attach to the ER in axonal growth cones and promote local translation in response to BDNF stimulation. (A) BDNF-stimulated motoneurons expressing mCherry–ER were stained for RPL24 and RPS6, and growth cones were imaged using SIM. White squares indicate regions of interest (ROIs) shown in magnified growth cone images on the right. (B) Graph shows co-cluster formation of RPL24 and RPS6 with the ER within 10 s and 1 min of BDNF stimulation (****P<0.0001; n=25–33 cells from three independent experiments). RPL24 and RPS6 co-clusters dissociate from the ER after long BDNF stimulation of 30 min (n.s., P=0.598; n=13 from two independent experiments). (C) CytoD-treated neurons do not show increased numbers of RPL24, RPS6 and ER co-clusters in growth cones in response to BDNF stimulation (n.s., P=0.728; n=30–32 cells from three independent experiments). (D) BDNF-stimulated motoneurons expressing mCherry–ER were stained using Y10B and anti-eEF2 antibodies, and growth cones were imaged using SIM. White squares indicate ROIs shown in magnified growth cone images on the right. (E) Graph shows co-cluster formation of Y10B and eEF2 with the ER within 10 s and 1 min BDNF stimulation (***P=0.0003; ****P<0.0001; n=23–27 cells from three independent experiments). Data in B,C,E are presented as scatter dot plots with mean±s.e.m. indicated. Statistical analyses used one-way ANOVA with Dunn's post-hoc test.

that motoneurons harbor RER in the axonal growth cone, which extends into filopodia and whose integrity and dynamic remodeling are regulated mainly by actin and myosin VI.

Unlike ER interactions with microtubules (Guo et al., 2018), the interaction of ER with the actin cytoskeleton, especially in the axonal growth cones where presynaptic structures form under specific culture conditions (Jablonka et al., 2007), is yet to be investigated in detail. In somatodendritic compartments, kinesin and dynein-based ER sliding along microtubules as well as interaction between STIM1 on the ER and EB1 (also known as MAPRE1) on the microtubule plus end have shown to mediate ER movements (Waterman-Storer and Salmon, 1998; Friedman et al., 2010). However, studies with cultured cells have revealed that (1) nocodazole treatment does not cause immediate retraction of the ER from the periphery (Terasaki et al., 1986), (2) ER tubules can form in the absence of microtubules (Dreier and Rapoport, 2000; Voeltz et al., 2006; Wang et al., 2013), and (3) disruption of actin filaments in hippocampal neurons affects Ca^{2+} release from the ER in soma (Wang et al., 2002). These observations indicate that ER dynamic movements might not depend only on microtubules but also on the actin cytoskeleton. Indeed, the first evidence for the role of actin in ER translocation into dendrites comes from a study by Wagner et al., showing that myosin Va, which is an actin-based motor, mediates ER movement in dendritic spines of Purkinje neurons (Wagner et al., 2011). Axonal growth cones consist of highly dynamic membrane protrusions – filopodia and lamellipodia – and a more stable central region called the growth cone core (Dent and Gertler, 2003). All these domains are transient and undergo constant growth and retraction in shape and structure (Dent et al., 2011). In contrast to the microtubule-rich core, actin is predominant in filopodia and lamellipodia. Therefore, dynamics of filopodia exceed those in the core (Mallavarapu and Mitchison, 1999; Bornschlögl et al., 2013). In line with this, our time-lapse recordings showed that the dynamics of the ER differ in the growth cone center and periphery. In the core of growth cones, the velocity of ER dynamic movements was much lower than that in actin-rich filopodia. Strikingly, actin depolymerization destroyed ER dynamic movements in filopodia of 80% of imaged cells. In addition, two-color live-cell imaging data revealed that the ER moves along actin in filopodia and that F-actin withdrawal results in nearly 99% retraction of ER from filopodia. Finally, pharmacological inhibition of myosin V and particularly of myosin VI significantly reduced the ER movements in filopodia, indicating that ER movements in the growth cone require myosin VI. These data provide the first direct evidence of an actin and myosin VI-dependent ER remodeling and integrity in axon terminals of neurons. ER entry into filopodia suggests a membrane contact site between the ER and the plasma membrane (Wu et al., 2017; Cohen et al., 2018). This physical tethering could be essential for the surface delivery of newly synthesized receptors, membrane proteins such as voltage-gated Ca^{2+} channels, as shown here, or lipids. Importantly, we found that ER movements in the core are regulated by both actin and microtubule cytoskeletons. Previous studies have demonstrated that F-actin and microtubules interact during neuronal polarization and development (Zhao et al., 2017; Dogterom and Koenderink, 2019; Meka et al., 2019). This crosstalk is mediated by macromolecules such as drebrin E, which physically links F-actin and microtubule plus end-binding proteins or other regulatory proteins, such as Rho GTPases, MAP2 and tau (Zhao et al., 2017; Dogterom and Koenderink, 2019). We show that knockdown of drebrin A significantly decreases the dynamic remodeling of axonal ER, indicating a role for this protein in the

coordinated actin and microtubule-based regulation of ER dynamics in axonal growth cones.

Subcellular control of axon growth, synapse differentiation and plasticity depend on regulatory mechanisms that ensure processing of local information and subsequent responses on a time scale of seconds. mRNA localization and local protein synthesis are conserved mechanisms that modify the axonal proteome at a fast temporal and short spatial scale, thereby maintaining the plasticity capacity of axonal synapses (Holt et al., 2019; Fernandopulle et al., 2021). In addition to cytoplasmic proteins, mRNAs encoding secreted and membrane proteins have been identified in axonal transcriptomes (Willis et al., 2007; Saal et al., 2014; Poulopoulos et al., 2019). On-site synthesis and glycosylation of such membrane proteins would require additional RER and Golgi machinery in the distal axon. However, previous studies have suggested that in axons the ER is devoid of ribosomes, and thus no direct evidence of its potential functions related to local protein synthesis has been reported yet (Tsukita and Ishikawa, 1976; Krijnse-Locker et al., 1995; Horton and Ehlers, 2003). Interestingly, Merianda et al. (2009) reported glycosylation patterns of transmembrane proteins being locally translated in axons of sensory neurons (Merianda et al., 2009). We tested the effects of a BDNF pulse in cultured motoneurons that were then investigated using super-resolution fluorescence imaging by SIM. This approach revealed that stimulation of motoneurons triggers the assembly of 80S ribosomes and initiates translation in axon terminals within 10 s. We observed that translationally active ribosomes attach to the ER in axonal growth cones, and local production of new proteins, including transmembrane proteins such as TrkB and α-1β subunits of N-type Ca^{2+} channels, becomes detectable within 1 min post stimulation. Contrary to axons, the response of soma to BDNF–TrkB activation was considerably slower and happened over longer time scales of several minutes. These distinctive response rates could be due to different intracellular levels of second messengers such as cAMP (Ming et al., 1997). It remains unknown whether similar or distinct signaling pathways downstream to BDNF–TrkB, such as mTOR, MAPK and PI3K pathways, are involved in activation of ribosomes and translation initiation in the growth cone and its counterparts. The rate of dynamic local translation at axonal terminals of cultured motoneurons appears relatively high. The fast and dynamic translocation of ribosomal subunits to ER that rapidly forms RER in axon terminals thus provides the basis for post-translational processing of locally synthesized proteins in response to extracellular stimuli. Intriguingly, 30 min after BDNF stimulation, 80S ribosomal subunits disassemble again and further dissociate from the ER, indicating that ribosomes only transiently associate with axonal ER in response to stimuli and explains why previous studies have failed to detect RER in axons using unstimulated neurons. Moreover, our data show that the rapid assembly of 80S ribosomes and their translocation toward the RER are disrupted upon pharmacological inhibition of actin assembly, suggesting involvement of an actin-based regulatory mechanism.

In summary, this work identifies a novel function for axonal ER in the regulation of stimulus-induced local translation and discloses a mechanism for dynamic regulation of the ER in axonal growth cones by a drebrin A-mediated actin and microtubule crosstalk.

MATERIALS AND METHODS
Animals
TrkB-knockout mice (Rohrer et al., 1999) were obtained from the University of California, Davis (MMRRC: 000188; B6; 129S4-*Ntrk2*^{tm1Rohr}), and were

maintained on a C57Bl/6 background. CD1 mice (Charles River Laboratories) were used for motoneuron cell cultures from wild-type mice. All mice were housed in the animal facility of the Institute of Clinical Neurobiology, University Hospital of Wuerzburg. All mouse procedures were performed according to the regulations on animal protection of the German federal law and of the Association for Assessment and Accreditation of Laboratory Animal care, approved by the local authorities.

Culture of embryonic mouse motoneurons

Embryonic mouse motoneuron culture was performed as previously described (Wiese et al., 2009). Lumbar spinal cords were dissected from CD1 mouse embryos at embryonic day (E)13.5, digested with trypsin (Worthington), triturated and then transferred onto a panning plate coated with anti-p75 antibody (MLR2, Abcam) for enrichment of motoneurons. For lentiviral transduction, lentiviruses expressing the pSIH-mCherry-KDEL construct were added to the suspension of motoneurons before plating on polyornithine- (PORN) and human merosin-coated (CC085, Merck-Millipore) plates. Merosin consists of laminin-211 ($\alpha2\beta1\gamma1$), enriched in extrasynaptic basal lamina and laminin-221 ($\alpha2\beta2\gamma1$), which is specifically expressed at the cleft of neuromuscular junctions (NMJs) and regulates formation, maturation and maintenance of NMJs (Fox et al., 2007; Rogers and Nishimune, 2017). Thus, culturing motoneurons on merosin induces the maturation of presynaptic structures in axon terminals. Motoneurons were cultured in NB medium (Thermo Fisher Scientific, 21103049) supplemented with 500 µM Glutamax (Thermo Fisher Scientific, 35050-038), 2% heat-inactivated horse serum (HS; Gibco), 2% B27 (Thermo Fisher Scientific) and 5 ng/ml BDNF (made in-house) for 5–6 days in a humidified CO_2 incubator at 37°C. Medium was changed 24 h after plating and then every other day. Compartmentalized motoneuron cultures were prepared as described previously (Saal et al., 2014). To drive axonal growth into the axonal compartment, 20 ng/ml BDNF and ciliary neurotrophic factor (CNTF; made in-house) were added into the axonal compartments, while only 5 ng/ml CNTF was added into the somatodendritic compartments.

Cloning and lentivirus production

For cloning of pSIH-mCherry-KDEL, mCherry was first amplified by PCR using a commercially available plasmid as template (Addgene, 61804; forward primer, 5′-ACTCGTCGACGTGAGCAAGGGCGAGGAGG-AT-3′; reverse primer, 5′-GAATGCGGCCGCCTTGTACAGCTCGTC-CATGCC-3′), and cut by SalI and NotI enzymes, followed by insertion into the pCMV-ECS2-CMV-myc-ER vector backbone (Samtleben et al., 2015) containing a KDEL sequence. The assembled mCherry–KDEL fragment was amplified by PCR from the above vector (forward primer, 5′-TTTGACCTCCATAGAAGATTCCACCATGGGATGGAGC-TG-3; reverse primer, 5′-TGTAATCCAGAGGTTGATTGCTACAGCT-CGTCCTTCTCG-3′), and the product was inserted into a lentiviral expression vector (pSIH-H1; System Biosciences, SI500A-1) containing a CMV promotor using NEBbuilder HIFI kit (New England Biolabs). To co-express GFP–actin and mCherry–KDEL, a previously described GFP–actin construct was used (Sivadasan et al., 2016). Both mCherry–KDEL and GFP–actin were first amplified by PCR, and purified fragments were inserted into a pSIH-CMV-IRES vector (Addgene, 110623). The expressed mCherry–KDEL fusion constructs are referred to throughout as mCherry–ER. To achieve knockdown of drebrin isoforms, shRNAs targeting mouse drebrin A and shRNAs targeting both drebrin A and drebrin E were cloned into a modified version of pSIH-H1 shRNA vector (System Biosciences) containing eGFP according to the manufacturer's instructions. The following antisense oligonucleotides were used: shDrebrin A, 5′-GTCCGTACTGCCCTTTCATAA-3′; shDrebrin A+E, 5′-GGCTGTGCTAACCTTCTTAAT-3′. Empty pSIH-H1 expressing eGFP was used as a control (shCtrl). Lentiviruses were produced in HEK[293T] cells (System Biosciences, 293TN Producer Cell Line) using pCMV-VSVG and pCMVΔR8.91 helper plasmids (Subramanian et al., 2012). HEK[293T] cells were transfected using calcium phosphate reagents, and viral supernatants were harvested after 47 h by ultracentrifugation at 76,653 **g** in a Beckman SW-32Ti rotor for 2 h at 4°C. NSC34 cells (Tebu-bio, CLU140-A) were used for a virus titer test as previously described (Subramanian et al., 2012).

qRT-PCR

Total RNA was extracted separately from somatodendritc and axonal compartments and reverse transcribed using random hexamers and Superscript III Reverse transcriptase enzyme (18080044; Invitrogen), as described previously (Moradi et al., 2017). cDNA was purified using a QIAGEN II purification kit (20021). For qRT-PCR, Luminaris HiGreen qPCR Master Mix (Thermo Fisher Scientific) was applied on a lightCycler 96 thermal cycler (Roche). Histone *H1f0* (also known as *H1-0*) transcripts were absent in RNA fractions obtained from axonal compartments, confirming the purity of mRNA preparation from these compartments. *Gapdh* was used for data normalization. The following primers were used for qRT-PCR: *TrkB*, 5′-CGGGAGCATCTCTCGGTCTAT-3′ (forward) and 5′-CTGGCAGAGTCATCGTCGTTG-3′ (reverse); *Gapdh*, 5′-AAC-TCCCACTCTTCCACCTTC-3′ (forward) and 5′-GGTCCAGGGTTTCT-TACTCCTT-3′ (reverse); and *H1f0*, 5′-CCCAAGTATTCAGACATGAT-3′ (forward) and 5′-CGCTTGATGGACAACT-3′ (reverse). To assess knockdown efficiency of shDrebrin A and shDrebrin A+E lentiviruses, primary motoneurons were transduced with knockdown lentiviral constructs and cultured for 7 days. Cells were first washed twice with RNAase-free phosphate-buffered saline (PBS) and then lysed in RNA lysis buffer. RNA was extracted using NucleoSpin RNA extraction kit (Macherey-Nagel) and reverse transcribed with random hexamers using a First Strand cDNA Synthesis Kit (Thermo Fisher Scientific). Reverse transcription reactions were diluted 1:5 in water and used for qRT-PCR. The following primers were used for qRT-PCR reactions: drebrin A forward, 5′-CCTGATAACC-CACGGGAGTT-3′; drebrin A reverse, 5′-GGAAGAGAGGTTTGGG-GTGC-3′; drebrin E forward, 5′-CCCACGGGAGTTCTTCAGACA-3′; drebrin E reverse, 5′-TCCAGGTGGCTGCATGGGAGGGAG-3′.

BDNF stimulation and immunocytochemistry of cultured motoneurons

After 6 days *in vitro* (DIV6), motoneurons were fixed with 4% paraformaldehyde (PFA) for 10 min at room temperature (RT) and permeabilized with 0.1% or 0.3% Triton X-100 for 10 min, followed by three washes with PBS. After incubation with block solution (10% donkey serum and 2% BSA in PBS) at RT for 1 h, primary antibodies were added and incubated at 4°C overnight. On the second day, motoneurons were washed thrice with PBS and incubated with secondary antibodies for 1 h, followed by another three washes. Aqua Poly/Mount (18606-20, Polysciences) was used for embedding. For β-actin staining, motoneurons were permeabilized with ice-cold methanol for 5 min at −20°C. For Cav2.2 staining, motoneurons were fixed with 4% PFA for 5 min at RT and permeabilized with 0.1% Triton X-100 in PBS for 5 min at RT. For the BDNF stimulation experiments, motoneurons were first cultured with 5 ng/ml BDNF. At DIV5, the medium was completely aspirated and cells were washed twice with NB medium to completely remove BDNF from all the surfaces. Cells were maintained in NB medium supplemented with 2% HS and 2% B27 overnight in the absence of neurotrophic factors. On the next day, BDNF stimulation was conducted by directly adding 40 ng/ml BDNF into the cell culture medium and cultures were kept on a 37°C hotplate. For different stimulation times, BDNF-containing medium was removed after 10 s, 1 min and 10 min stimulation, and 4% PFA was directly added onto cells. For the no BDNF control group, the same amount of NB medium without BDNF was added. The following primary antibodies were used: monoclonal mouse anti-α-tubulin (T5168, Sigma-Aldrich; 1:1000), polyclonal goat anti-TrkB (AF1494, Bio-Techne Sales Corp; 1:500), monoclonal mouse anti-rRNA (Y10b) (MA116628, Thermo Fisher Scientific; 1:500), polyclonal goat anti-ribosomal protein L8 (SAB2500882, Sigma-Aldrich; 1:500), monoclonal mouse anti-β-actin (GTX26276, GeneTex; 1:1000), polyclonal rabbit anti-tau (T6402, Sigma-Aldrich; 1:1000), polyclonal rabbit anti-eEF2 (23325, Cell Signaling Technology; 1:50), monoclonal mouse anti-S6 ribosomal protein (MA515123, Thermo Fisher Scientific; 1:100), polyclonal rabbit anti-RPL24 (PA530157, Thermo Fisher Scientific; 1:500), polyclonal guinea pig antiserum RFP (390004, Synaptic Systems; 1:500), polyclonal guinea pig Ca^{2+} channel N-type alpha-1B channel (152305, Synaptic Systems, 1:250) and monoclonal rat anti-mCherry (M11217, Thermo Fisher Scientific; 1:1500). Secondary antibodies: donkey anti-mouse IgG (H+L)

(Alexa Fluor 488; A21202, Life Technologies), donkey anti-rabbit IgG (H+l) AffiniPure (Alexa Fluor 488; 711-545-152, Jackson ImmunoResearch), donkey anti-guinea pig IgG (H+L) AffiniPure (Cy3; 706-165-148, Jackson ImmunoResearch), donkey anti-rat IgG (H+L) AffiniPure (Cy3; 712-165-150, Jackson ImmunoResearch), donkey anti-rabbit IgG (H+L) AffiniPure (Cy3; 711-165-152, Jackson ImmunoResearch), donkey anti-goat IgG (H+L) AffiniPure (Cy3; 705-165-147, Jackson ImmunoResearch), donkey anti-mouse IgG (H+L) (Cy3; 715-165-151, Jackson ImmunoResearch; 1:500), donkey anti-goat IgG (H+L) AffiniPure (Alexa Fluor 647; 705-605-003, Jackson ImmunoResearch), donkey anti-mouse IgG (H+L) highly cross-adsorbed (Alexa Fluor 647; A31571, Invitrogen), donkey anti-rabbit IgG (H+L) AffiniPure (Cy5; 711-175-152, Jackson ImmunoResearch). F-actin was labeled with Alexa Fluor 647-conjugated Phalloidin (A22287; Invitrogen). All secondary antibodies were diluted 1:500 in Tris-buffered saline containing 0.1% Tween (TBST).

Puromycin experiments
Motoneurons were incubated with 10 μg/ml puromycin (Merck, P8833) for 10 min, and BDNF stimulation was carried out as described in the above section. Cells were then fixed and immunostained using anti-puromycin immunostaining. Nocodazole (Merck, M1404) was used to disrupt microtubule-dependent axonal transport and anisomycin (Merck, 176880) was used as translational inhibitor. Cells were treated with 10 μM nocodazole for 2 h and 100 ng/ml anisomycin for 1 h prior to as well as during puromycin incubation followed by BDNF stimulation. Primary and secondary antibodies used were: monoclonal mouse anti-puromycin (clone 12D10, MABE343, Merck Millipore; 1:1000), polyclonal rabbit anti-tau (T6402, Sigma-Aldrich; 1:1000), donkey anti-mouse IgG (H+L) (Alexa Fluor 488; A21202, Life Technologies; 1:500) and donkey anti-rabbit IgG (H+L) AffiniPure (Cy3; 711-165-152; Jackson ImmunoResearch; 1:500).

Image acquisition and data analysis
Image acquisition was performed with a standard Olympus Fluoview 1000 confocal system with a 60× NA 1.35 oil objective. Structured illumination microscopy (SIM) imaging was performed on a commercial ELYRA S.1 microscope (Zeiss AG). The setup is equipped with a Plan-Apochromat 63× NA 1.40 immersion-oil based objective and four excitation lasers: a 405 nm diode (50 mW), a 488 nm OPSL (100 mW), a 561 nm OPSL (100 mW) and a 642 nm diode laser (150 mW). 3D reconstruction was performed using Imaris software (Oxford Instruments). For quantification of immunofluorescence signals, mean gray values of images were measured from unprocessed raw data after background subtraction using ImageJ-win64 (NIH, Bethesda, MD, USA). For quantification of SIM data represented in Figs 4 and 4, co-clusters of RPL24/RPS6, Y10B/eEF2 as well as RPL24/RPS6/ER and Y10B/eEF2/ER were counted manually. For this, maximum projections of single SIM channels (RPL24, RPS6 and mCherry–ER or Y10B, eEF2 and mCherry–ER channels) were first created using ImageJ. An automatic linear adjustment of contrast and brightness was applied to the whole z-projection image of each single channel and these were merged into an RGB image. Co-clusters were defined as overlapping dots from RPL24, RPS6 and mCherry–ER channels or Y10B, eEF2 and mCherry–ER channels on the RGB image that had a diameter of more than 350 nm. In addition, colocalization of RPL24/RPS6 as well as Y10B/eEF2 shown in Fig. 4 was assessed by Pearson's correlation coefficient using the Coloc2 plugin of Fiji (https://fiji.sc/). GraphPad Prism 9 software was used for all statistical analyses. Data are shown in scatter dot plots with mean±s.e.m., unless otherwise mentioned. For better visibility, linear contrast enhancement was applied to all representative images using Adobe Photoshop.

Live-cell imaging and data quantification
Approximately 40,000 motoneurons were transduced with lentivirus expressing pSIH-mCherry-KDEL or pSIH-GFP-actin-IRES-mCherry-KDEL and cultured on PORN- and merosin-coated 35 mm high μ-dishes (81156, IBIDI) for 6 days. For pharmacological treatments, cytochalasin D (Sigma-Aldrich; C2618), nocodazole (Sigma-Aldrich; M1404), (−)-blebbistatin (Sigma-Aldrich; B0560), MyoVin-1 (Calbiochem;

475984) and 2,4,6-triiodophenol (Sigma-Aldrich; 137723) were dissolved and diluted in DMSO (PanReac AppliChem). Cells were treated at the following concentration and incubation time before live-cell imaging: 1 μg/ml cytochalasin D for 30 min; 10 μM nocodazole for 2 h; 5 μM (−)-blebbistatin for 15 min; 30 μM MyoVin-1 for 15 min and 1 μM 2,4,6-triiodophenol for 15 min. For live-cell imaging, cells were washed twice with pre-warmed Tyrode's solution (125 mM NaCl, 2 mM KCl, 2 mM CaCl$_2$, 2 mM MgCl$_2$, 30 mM glucose and 25 mM HEPES, pH 7.4) and subsequently imaged in 2 ml Tyrode's solution. Imaging was performed using an inverted epifluorescence microscope (TE2000; Nikon) that was equipped with a perfect focus system, heated stage chamber (TOKAI HIT CO, LTD) at 37°C and 5% CO2, and a 60×1.4 NA objective. Time series were captured at a speed of 2 s per frame over 15 min. 12-bit images of 1024×1024 pixels were acquired with an Orca Flash 4.0 V2 camera (Hamamatsu Photonics), controlled by Nikon Element image software. For quantification of ER dynamics, image correlation spectroscopy (ICS; Wiseman, 2015) was implemented using Python. This approach was used as described previously by Wiseman (2015). Briefly, molecular movements of ER or molecular transport of other organelles are determined based on flow or diffusion in an image time series $\{I\}_{i,j,t}^{N,M,T}$, with N, M and T indicating the two dimensions in space and the time dimension, respectively. i, j, t denote the corresponding running indices that the basic workflow starts by defining a space–time window, i.e. a subspace of $K=L=10$ pixels over $\Delta t=10$ consecutive frames. This subspace is rasterized over the image with a sampling rate of $\Delta i=\Delta j=4$. For each of those samples, a correlation window $\{C\}_{x,y}^{K,L}$ is computed, describing the overlap of signal for a given shift x, y per time frame. The maximum of this spectrum is the point of maximum correlation and indicates a shift of signal from one image to this next, by: $(\Delta i, \Delta j)=(x_{max}-K/2, y_{max}-L/2)$.

To achieve sub-pixel accuracy, a 2D Gaussian function is fitted to the correlation spectrum using the Levenberg–Marquardt algorithm. The initial parameters were chosen as: amplitude, $A=max(C)$; center coordinates in x, $x_0=K/2$; center coordinates in y, $y_0=L/2$; standard deviation in x, $\sigma_x=K/4$; and standard deviation in y, $\sigma_y=L/4$. An additional parameter θ, rotating the coordinate system by θ, was initialized as 0. The fitted results for x_0 and y_0 indicate a directed shift of signal. A larger σ_x or σ_y indicates an overall lower correlation, i.e. the signal losing its shape. To compute overall dynamics, three distinct subspaces are classified: (1) subspaces with a mean intensity less than 10% of the maximum intensity, which are considered noise; (2) subspaces with a mean intensity that is larger than 40% of the maximum intensity, which are classified as core; and (3) subspaces with an intensity of 10–40% of the maximum intensity, which are classified as filopodia. The overall dynamics value for a class is the mean dynamics value of all subspaces. Kymograph analysis of ER dynamics was carried out using ImageJ as described previously (Moradi et al., 2017). Briefly, a z-projection image was made from all the frames of a live-cell image, followed by the creation of a multiple kymograph along a line drawn tracking the ER movements in the filopodia or core. Distance changed per movement and frequency of movements over 15 min were calculated from multiple kymographs and plotted in a graph. Growth cones without detectable ER movements were classified as failures in filopodia or core ER movement.

Western blotting
For western blot analysis, ∼300,000 motoneurons were plated onto a PORN- and merosin-coated 24-well cell culture dish. At DIV6, BDNF-deprived neurons were stimulated with 40 ng/ml BDNF for 10 s, 30 s, 1 min and 10 min, and cells were lysed directly in 2× Laemmli buffer (125 mM Tris-HCl, pH 6.8, 10% SDS, 50% glycerol, 25% β-mercaptoethanol and 0.2% Bromophenol Blue). The protein lysates were boiled at 99°C for 10 min. Protein extracts were separated using 4–12% gradient SDS-PAGE gels. Proteins were then blotted onto nitrocellulose membranes, and primary antibodies were incubated on a shaker at 4°C overnight. Primary antibodies were washed with TBST, and secondary antibodies were incubated at RT for 1 h, washed in TBST and developed using ECL systems (GE Healthcare). The primary antibodies used were monoclonal rabbit anti-pTrkA/B (Cell Signaling Technology, 4619; 1:500), polyclonal goat anti-TrkB (AF1494, Bio-Techne Sales Corp; 1:500) and monoclonal mouse anti-α-tubulin (T5168, Sigma-Aldrich; 1:5000). The secondary antibodies used were

peroxidase-conjugated AffiniPure donkey anti-rabbit IgG (H+L) (711-035-152, Jackson ImmunoResearch; 1:10,000), peroxidase-conjugated AffiniPure donkey anti-goat IgG (H+L) (705-035-003, Jackson ImmunoResearch; 1:10,000) and peroxidase-conjugated AffiniPure goat anti-mouse IgG (H+L) (115-035-146, Jackson ImmunoResearch; 1:10,000).

References

Ben-Shem, A., Garreau de Loubresse, N., Melnikov, S., Jenner, L., Yusupova, G. and Yusupov, M. (2011). The structure of the eukaryotic ribosome at 3.0 A resolution. *Science* **334**, 1524-1529. doi:10.1126/science.1212642

Biever, A., Glock, C., Tushev, G., Ciirdaeva, E., Dalmay, T., Langer, J. D. and Schuman, E. M. (2020). Monosomes actively translate synaptic mRNAs in neuronal processes. *Science* **367**, eaay4991. doi:10.1126/science.aay4991

Blackstone, C. (2012). Cellular pathways of hereditary spastic paraplegia. *Annu. Rev. Neurosci.* **35**, 25-47. doi:10.1146/annurev-neuro-062111-150400

Bornschlögl, T., Romero, S., Vestergaard, C. L., Joanny, J. F., Van Nhieu, G. T. and Bassereau, P. (2013). Filopodial retraction force is generated by cortical actin dynamics and controlled by reversible tethering at the tip. *Proc. Natl. Acad. Sci. USA* **110**, 18928-18933. doi:10.1073/pnas.1316572110

Briese, M., Saal, L., Appenzeller, S., Moradi, M., Baluapuri, A. and Sendtner, M. (2016). Whole transcriptome profiling reveals the RNA content of motor axons. *Nucleic Acids Res.* **44**, e33. doi:10.1093/nar/gkv1027

Cohen, S., Valm, A. M. and Lippincott-Schwartz, J. (2018). Interacting organelles. *Curr. Opin. Cell Biol.* **53**, 84-91. doi:10.1016/j.ceb.2018.06.003

Dailey, M. and Bridgman, P. (1989). Dynamics of the endoplasmic reticulum and other membranous organelles in growth cones of cultured neurons. *J. Neurosci.* **9**, 1897-1909. doi:10.1523/JNEUROSCI.09-06-01897.1989

De Gregorio, C., Delgado, R., Ibacache, A., Sierralta, J. and Couve, A. (2017). Drosophila Atlastin in motor neurons is required for locomotion and presynaptic function. *J. Cell Sci.* **130**, 3507-3516. doi:10.1242/jcs.201657

Dent, E. W. and Gertler, F. B. (2003). Cytoskeletal dynamics and transport in growth cone motility and axon guidance. *Neuron* **40**, 209-227. doi:10.1016/S0896-6273(03)00633-0

Dent, E. W., Gupton, S. L. and Gertler, F. B. (2011). The growth cone cytoskeleton in axon outgrowth and guidance. *Cold Spring Harb. Perspect Biol.* **3**, a001800. doi:10.1101/cshperspect.a001800

Dogterom, M. and Koenderink, G. H. (2019). Actin-microtubule crosstalk in cell biology. *Nat. Rev. Mol. Cell Biol.* **20**, 38-54. doi:10.1038/s41580-018-0067-1

Dreier, L. and Rapoport, T. A. (2000). In vitro formation of the endoplasmic reticulum occurs independently of microtubules by a controlled fusion reaction. *J. Cell Biol.* **148**, 883-898. doi:10.1083/jcb.148.5.883

Du, Y., Walker, L., Novick, P. and Ferro-Novick, S. (2006). Ptc1p regulates cortical ER inheritance via Slt2p. *EMBO J.* **25**, 4413-4422. doi:10.1038/sj.emboj.7601319

Farah, C. A., Liazoghli, D., Perreault, S., Desjardins, M., Guimont, A., Anton, A., Lauzon, M., Kreibich, G., Paiement, J. and Leclerc, N. (2005). Interaction of microtubule-associated protein-2 and p63: a new link between microtubules and rough endoplasmic reticulum membranes in neurons. *J. Biol. Chem.* **280**, 9439-9449. doi:10.1074/jbc.M412304200

Farias, G. G., Freal, A., Tortosa, E., Stucchi, R., Pan, X., Portegies, S., Will, L., Altelaar, M. and Hoogenraad, C. C. (2019). Feedback-driven mechanisms between microtubules and the endoplasmic reticulum instruct neuronal polarity. *Neuron* **102**, 184-201.e188. doi:10.1016/j.neuron.2019.01.030

Fernandopulle, M. S., Lippincott-Schwartz, J. and Ward, M. E. (2021). RNA transport and local translation in neurodevelopmental and neurodegenerative disease. *Nat. Neurosci.* **24**, 622-632. doi:10.1038/s41593-020-00785-2

Fox, M. A., Sanes, J. R., Borza, D. B., Eswarakumar, V. P., Fässler, R., Hudson, B. G., John, S. W., Ninomiya, Y., Pedchenko, V., Pfaff, S. L. et al. (2007). Distinct target-derived signals organize formation, maturation, and maintenance of motor nerve terminals. *Cell* **129**, 179-193. doi:10.1016/j.cell.2007.02.035

Friedman, J. R., Webster, B. M., Mastronarde, D. N., Verhey, K. J. and Voeltz, G. K. (2010). ER sliding dynamics and ER-mitochondrial contacts occur on acetylated microtubules. *J. Cell Biol.* **190**, 363-375. doi:10.1083/jcb.200911024

Geraldo, S. and Gordon-Weeks, P. R. (2009). Cytoskeletal dynamics in growth-cone steering. *J. Cell Sci.* **122**, 3595-3604. doi:10.1242/jcs.042309

Geraldo, S., Khanzada, U. K., Parsons, M., Chilton, J. K. and Gordon-Weeks, P. R. (2008). Targeting of the F-actin-binding protein drebrin by the microtubule plus-tip protein EB3 is required for neuritogenesis. *Nat. Cell Biol.* **10**, 1181-1189. doi:10.1038/ncb1778

Griffing, L. R. (2010). Networking in the endoplasmic reticulum. *Biochem. Soc. Trans.* **38**, 747-753. doi:10.1042/BST0380747

Guo, Y., Li, D., Zhang, S., Yang, Y., Liu, J.-J., Wang, X., Liu, C., Milkie, D. E., Moore, R. P., Tulu, U. S. et al. (2018). Visualizing intracellular organelle and cytoskeletal interactions at nanoscale resolution on millisecond timescales. *Cell* **175**, 1430-1442.e1417. doi:10.1016/j.cell.2018.09.057

Holt, C. E., Martin, K. C. and Schuman, E. M. (2019). Local translation in neurons: visualization and function. *Nat. Struct. Mol. Biol.* **26**, 557-566. doi:10.1038/s41594-019-0263-5

Horton, A. C. and Ehlers, M. D. (2003). Dual modes of endoplasmic reticulum-to-Golgi transport in dendrites revealed by live-cell imaging. *J. Neurosci.* **23**, 6188-6199. doi:10.1523/JNEUROSCI.23-15-06188.2003

Hua, Z., Gu, X., Dong, Y., Tan, F., Liu, Z., Thiele, C. J. and Li, Z. (2016). PI3K and MAPK pathways mediate the BDNF/TrkB-increased metastasis in neuroblastoma. *Tumour Biol.* **37**, 16227-16236. doi:10.1007/s13277-016-5433-z

Huang, E. J. and Reichardt, L. F. (2003). Trk receptors: roles in neuronal signal transduction. *Annu. Rev. Biochem.* **72**, 609-642. doi:10.1146/annurev.biochem.72.121801.161629

Jablonka, S., Beck, M., Lechner, B. D., Mayer, C. and Sendtner, M. (2007). Defective Ca2+ channel clustering in axon terminals disturbs excitability in motoneurons in spinal muscular atrophy. *J. Cell Biol.* **179**, 139-149. doi:10.1083/jcb.200703187

Krijnse-Locker, J., Parton, R. G., Fuller, S. D., Griffiths, G. and Dotti, C. G. (1995). The organization of the endoplasmic reticulum and the intermediate compartment in cultured rat hippocampal neurons. *Mol. Biol. Cell* **6**, 1315-1332. doi:10.1091/mbc.6.10.1315

Leal, G., Comprido, D. and Duarte, C. B. (2014). BDNF-induced local protein synthesis and synaptic plasticity. *Neuropharmacology* **76**, 639-656. doi:10.1016/j.neuropharm.2013.04.005

Lee, J. E., Cathey, P. I., Wu, H., Parker, R. and Voeltz, G. K. (2020). Endoplasmic reticulum contact sites regulate the dynamics of membraneless organelles. *Science* **367**, 6477. doi:10.1126/science.aay7108

Leung, K. M., van Horck, F. P., Lin, A. C., Allison, R., Standart, N. and Holt, C. E. (2006). Asymmetrical beta-actin mRNA translation in growth cones mediates attractive turning to netrin-1. *Nat. Neurosci.* **9**, 1247-1256. doi:10.1038/nn1775

Lindhout, F. W., Cao, Y., Kevenaar, J. T., Bodzeta, A., Stucchi, R., Boumpoutsari, M. M., Katrukha, E. A., Altelaar, M., MacGillavry, H. D. and Hoogenraad, C. C. (2019). VAP-SCRN1 interaction regulates dynamic endoplasmic reticulum remodeling and presynaptic function. *EMBO J.* **38**, e101345. doi:10.15252/embj.2018101345

Lu, L., Ladinsky, M. S. and Kirchhausen, T. (2009). Cisternal organization of the endoplasmic reticulum during mitosis. *Mol. Biol. Cell* **20**, 3471-3480. doi:10.1091/mbc.e09-04-0327

Maday, S., Twelvetrees, A. E., Moughamian, A. J. and Holzbaur, E. L. (2014). Axonal transport: cargo-specific mechanisms of motility and regulation. *Neuron* **84**, 292-309. doi:10.1016/j.neuron.2014.10.019

Mallavarapu, A. and Mitchison, T. (1999). Regulated actin cytoskeleton assembly at filopodium tips controls their extension and retraction. *J. Cell Biol.* **146**, 1097-1106. doi:10.1083/jcb.146.5.1097

Meka, D. P., Scharrenberg, R., Zhao, B., Kobler, O., Konig, T., Schaefer, I., Schwanke, B., Klykov, S., Richter, M., Eggert, D. et al. (2019). Radial somatic F-actin organization affects growth cone dynamics during early neuronal development. *EMBO Rep.* **20**, e47743.

Merianda, T. T., Lin, A. C., Lam, J. S., Vuppalanchi, D., Willis, D. E., Karin, N., Holt, C. E. and Twiss, J. L. (2009). A functional equivalent of endoplasmic reticulum and Golgi in axons for secretion of locally synthesized proteins. *Mol. Cell. Neurosci.* **40**, 128-142. doi:10.1016/j.mcn.2008.09.008

Ming, G. L., Song, H. J., Berninger, B., Holt, C. E., Tessier-Lavigne, M. and Poo, M. M. (1997). cAMP-dependent growth cone guidance by netrin-1. *Neuron* **19**, 1225-1235. doi:10.1016/S0896-6273(00)80414-6

Moradi, M., Sivadasan, R., Saal, L., Luningschror, P., Dombert, B., Rathod, R. J., Dieterich, D. C., Blum, R. and Sendtner, M. (2017). Differential roles of alpha-, beta-, and gamma-actin in axon growth and collateral branch formation in motoneurons. *J. Cell Biol.* **216**, 793-814. doi:10.1083/jcb.201604117

Öztürk, Z., O'Kane, C. J. and Pérez-Moreno, J. J. (2020). Axonal Endoplasmic Reticulum Dynamics and Its Roles in Neurodegeneration. *Front. Neurosci.* **14**, 48. doi:10.3389/fnins.2020.00048

Poulopoulos, A., Murphy, A. J., Ozkan, A., Davis, P., Hatch, J., Kirchner, R. and Macklis, J. D. (2019). Subcellular transcriptomes and proteomes of developing axon projections in the cerebral cortex. *Nature* **565**, 356-360. doi:10.1038/s41586-018-0847-y

Prinz, W. A., Grzyb, L., Veenhuis, M., Kahana, J. A., Silver, P. A. and Rapoport, T. A. (2000). Mutants affecting the structure of the cortical endoplasmic reticulum in Saccharomyces cerevisiae. *J. Cell Biol.* **150**, 461-474. doi:10.1083/jcb.150.3.461

Puhka, M., Joensuu, M., Vihinen, H., Belevich, I. and Jokitalo, E. (2012). Progressive sheet-to-tubule transformation is a general mechanism for endoplasmic reticulum partitioning in dividing mammalian cells. *Mol. Biol. Cell* **23**, 2424-2432. doi:10.1091/mbc.e10-12-0950

Rathod, R., Havlicek, S., Frank, N., Blum, R. and Sendtner, M. (2012). Laminin induced local axonal translation of beta-actin mRNA is impaired in SMN-deficient motoneurons. *Histochem. Cell Biol.* **138**, 737-748. doi:10.1007/s00418-012-0989-1

Rogers, R. S. and Nishimune, H. (2017). The role of laminins in the organization and function of neuromuscular junctions. *Matrix Biol.* **57-58**, 86-105. doi:10.1016/j.matbio.2016.08.008

Rohrer, B., Korenbrot, J. I., LaVail, M. M., Reichardt, L. F. and Xu, B. (1999). Role of neurotrophin receptor TrkB in the maturation of rod photoreceptors and establishment of synaptic transmission to the inner retina. *J. Neurosci.* **19**, 8919-8930. doi:10.1523/JNEUROSCI.19-20-08919.1999

Saal, L., Briese, M., Kneitz, S., Glinka, M. and Sendtner, M. (2014). Subcellular transcriptome alterations in a cell culture model of spinal muscular atrophy point to widespread defects in axonal growth and presynaptic differentiation. *RNA* **20**, 1789-1802. doi:10.1261/rna.047373.114

Samtleben, S., Wachter, B. and Blum, R. (2015). Store-operated calcium entry compensates fast ER calcium loss in resting hippocampal neurons. *Cell Calcium* **58**, 147-159. doi:10.1016/j.ceca.2015.04.002

Santos, A. R., Comprido, D. and Duarte, C. B. (2010). Regulation of local translation at the synapse by BDNF. *Prog. Neurobiol.* **92**, 505-516. doi:10.1016/j.pneurobio.2010.08.004

Sasaki, Y., Welshhans, K., Wen, Z., Yao, J., Xu, M., Goshima, Y., Zheng, J. Q. and Bassell, G. J. (2010). Phosphorylation of zipcode binding protein 1 is required for brain-derived neurotrophic factor signaling of local beta-actin synthesis and growth cone turning. *J. Neurosci.* **30**, 9349-9358. doi:10.1523/JNEUROSCI.0499-10.2010

Shibata, Y., Shemesh, T., Prinz, W. A., Palazzo, A. F., Kozlov, M. M. and Rapoport, T. A. (2010). Mechanisms determining the morphology of the peripheral ER. *Cell* **143**, 774-788. doi:10.1016/j.cell.2010.11.007

Shirao, T., Hanamura, K., Koganezawa, N., Ishizuka, Y., Yamazaki, H. and Sekino, Y. (2017). The role of drebrin in neurons. *J. Neurochem.* **141**, 819-834. doi:10.1111/jnc.13988

Sivadasan, R., Hornburg, D., Drepper, C., Frank, N., Jablonka, S., Hansel, A., Lojewski, X., Sterneckert, J., Hermann, A., Shaw, P. J. et al. (2016). C9ORF72 interaction with cofilin modulates actin dynamics in motor neurons. *Nat. Neurosci.* **19**, 1610-1618. doi:10.1038/nn.4407

Subramanian, N., Wetzel, A., Dombert, B., Yadav, P., Havlicek, S., Jablonka, S., Nassar, M. A., Blum, R. and Sendtner, M. (2012). Role of Nav1.9 in activity-dependent axon growth in motoneurons. *Hum. Mol. Genet.* **21**, 3655-3667. doi:10.1093/hmg/dds195

Summerville, J. B., Faust, J. F., Fan, E., Pendin, D., Daga, A., Formella, J., Stern, M. and McNew, J. A. (2016). The effects of ER morphology on synaptic structure and function in Drosophila melanogaster. *J. Cell Sci.* **129**, 1635-1648. doi:10.1242/jcs.184929

Terasaki, M., Slater, N. T., Fein, A., Schmidek, A. and Reese, T. S. (1994). Continuous network of endoplasmic reticulum in cerebellar Purkinje neurons. *Proc. Natl. Acad. Sci. USA* **91**, 7510-7514. doi:10.1073/pnas.91.16.7510

Terasaki, M., Chen, L. B. and Fujiwara, K. (1986). Microtubules and the endoplasmic reticulum are highly interdependent structures. *J. Cell Biol.* **103**, 1557-1568. doi:10.1083/jcb.103.4.1557

Terenzio, M., Koley, S., Samra, N., Rishal, I., Zhao, Q., Sahoo, P. K., Urisman, A., Marvaldi, L., Oses-Prieto, J. A., Forester, C. et al. (2018). Locally translated mTOR controls axonal local translation in nerve injury. *Science* **359**, 1416-1421. doi:10.1126/science.aan1053

Teuling, E., Ahmed, S., Haasdijk, E., Demmers, J., Steinmetz, M. O., Akhmanova, A., Jaarsma, D. and Hoogenraad, C. C. (2007). Motor neuron disease-associated mutant vesicle-associated membrane protein-associated protein (VAP) B recruits wild-type VAPs into endoplasmic reticulum-derived tubular aggregates. *J. Neurosci.* **27**, 9801-9815. doi:10.1523/JNEUROSCI.2661-07.2007

Trivedi, N., Stabley, D. R., Cain, B., Howell, D., Laumonnerie, C., Ramahi, J. S., Temirov, J., Kerekes, R. A., Gordon-Weeks, P. R. and Solecki, D. J. (2017). Drebrin-mediated microtubule–actomyosin coupling steers cerebellar granule neuron nucleokinesis and migration pathway selection. *Nat. Commun.* **8**, 14484. doi:10.1038/ncomms14484

Tsai, N. P., Bi, J., Loh, H. H. and Wei, L. N. (2006). Netrin-1 signaling regulates de novo protein synthesis of kappa opioid receptor by facilitating polysomal partition of its mRNA. *J. Neurosci.* **26**, 9743-9749. doi:10.1523/JNEUROSCI.3014-06.2006

Tsukita, S. and Ishikawa, H. (1976). Three-dimensional distribution of smooth endoplasmic reticulum in myelinated axons. *J Electron Microsc (Tokyo)* **25**, 141-149.

Voeltz, G. K., Prinz, W. A., Shibata, Y., Rist, J. M. and Rapoport, T. A. (2006). A class of membrane proteins shaping the tubular endoplasmic reticulum. *Cell* **124**, 573-586. doi:10.1016/j.cell.2005.11.047

Wagner, W., Brenowitz, S. D. and Hammer, J. A.III. (2011). Myosin-Va transports the endoplasmic reticulum into the dendritic spines of Purkinje neurons. *Nat. Cell Biol.* **13**, 40-48. doi:10.1038/ncb2132

Wang, Y., Mattson, M. P. and Furukawa, K. (2002). Endoplasmic reticulum calcium release is modulated by actin polymerization. *J. Neurochem.* **82**, 945-952. doi:10.1046/j.1471-4159.2002.01059.x

Wang, S., Romano, F. B., Field, C. M., Mitchison, T. J. and Rapoport, T. A. (2013). Multiple mechanisms determine ER network morphology during the cell cycle in Xenopus egg extracts. *J. Cell Biol.* **203**, 801-814. doi:10.1083/jcb.201308001

Waterman-Storer, C. M. and Salmon, E. D. (1998). Endoplasmic reticulum membrane tubules are distributed by microtubules in living cells using three distinct mechanisms. *Curr. Biol.* **8**, 798-806. doi:10.1016/S0960-9822(98)70321-5

West, M., Zurek, N., Hoenger, A. and Voeltz, G. K. (2011). A 3D analysis of yeast ER structure reveals how ER domains are organized by membrane curvature. *J. Cell Biol.* **193**, 333-346. doi:10.1083/jcb.201011039

Wiese, S., Herrmann, T., Drepper, C., Jablonka, S., Funk, N., Klausmeyer, A., Rogers, M.-L., Rush, R. and Sendtner, M. (2009). Isolation and enrichment of embryonic mouse motoneurons from the lumbar spinal cord of individual mouse embryos. *Nat. Protoc.* **5**, 31-38. doi:10.1038/nprot.2009.193

Willis, D., Li, K. W., Zheng, J. Q., Chang, J. H., Smit, A. B., Kelly, T., Merianda, T. T., Sylvester, J., van Minnen, J. and Twiss, J. L. (2005). Differential transport and local translation of cytoskeletal, injury-response, and neurodegeneration protein mRNAs in axons. *J. Neurosci.* **25**, 778-791. doi:10.1523/JNEUROSCI.4235-04.2005

Willis, D. E., van Niekerk, E. A., Sasaki, Y., Mesngon, M., Merianda, T. T., Williams, G. G., Kendall, M., Smith, D. S., Bassell, G. J. and Twiss, J. L. (2007). Extracellular stimuli specifically regulate localized levels of individual neuronal mRNAs. *J. Cell Biol.* **178**, 965-980. doi:10.1083/jcb.200703209

Wiseman, P. W. (2015). Image correlation spectroscopy: principles and applications. *Cold Spring Harb. Protoc.* **2015**, 336-348. doi:10.1101/pdb.top086124

Worth, D. C., Daly, C. N., Geraldo, S., Oozeer, F. and Gordon-Weeks, P. R. (2013). Drebrin contains a cryptic F-actin-bundling activity regulated by Cdk5 phosphorylation. *J. Cell Biol.* **202**, 793-806. doi:10.1083/jcb.201303005

Wortman, J. C., Shrestha, U. M., Barry, D. M., Garcia, M. L., Gross, S. P. and Yu, C. C. (2014). Axonal transport: how high microtubule density can compensate for boundary effects in small-caliber axons. *Biophys. J.* **106**, 813-823. doi:10.1016/j.bpj.2013.12.047

Wozniak, M. J., Bola, B., Brownhill, K., Yang, Y. C., Levakova, V. and Allan, V. J. (2009). Role of kinesin-1 and cytoplasmic dynein in endoplasmic reticulum movement in VERO cells. *J. Cell Sci.* **122**, 1979-1989. doi:10.1242/jcs.041962

Wu, Y., Whiteus, C., Xu, C. S., Hayworth, K. J., Weinberg, R. J., Hess, H. F. and De Camilli, P. (2017). Contacts between the endoplasmic reticulum and other membranes in neurons. *Proc. Natl. Acad. Sci. USA* **114**, E4859-E4867. doi:10.1073/pnas.1701078114

Yoon, B. C., Zivraj, K. H. and Holt, C. E. (2009). Local translation and mRNA trafficking in axon pathfinding. *Results Probl. Cell Differ.* **48**, 269-288. doi:10.1007/400_2009_5

Zhao, B., Meka, D. P., Scharrenberg, R., Konig, T., Schwanke, B., Kobler, O., Windhorst, S., Kreutz, M. R., Mikhaylova, M. and Calderon de Anda, F. (2017). Microtubules modulate F-actin dynamics during neuronal polarization. *Sci. Rep.* **7**, 9583. doi:10.1038/s41598-017-09832-8